Boussinesq Models and Applications to Nearshore Wave Propagation, Surfzone Processes and Wave-Induced Currents

by

James T. Kirby

To appear in:
Advances in Coastal Engineering
V. C. Lakhan (ed)

This research supported by
National Oceanographic Partnership Program

RESEARCH REPORT NO. CACR-02-03
August, 2002

Center for Applied Coastal Research
Ocean Engineering Laboratory
University of Delaware
Newark, DE 19716

Boussinesq Models and Applications to Nearshore Wave Propagation, Surfzone Processes and Wave-Induced Currents

James T. Kirby
Center for Applied Coastal Research, University of Delaware
Newark, DE 19716, USA, kirby@udel.edu

1 Introduction

Classical Boussinesq theory provides a set of evolution equations for surface water waves in the combined limit of weak nonlinearity (characterized by $\delta \ll 1$) and weak dispersion ($\mu \ll 1$) with the ratio $\delta/\mu^2 = O(1)$. The parameters represent a wave height to water depth ratio, and a water depth to wavelength ratio, respectively. In an early review of the state of modeling efforts directed at predicting wave-induced nearshore circulation, Basco (1983) concluded that

> "The Boussinesq theory offers the possibility to eventually raise the fundamental knowledge of coastal hydrodynamics to a higher level. No time-averaging is involved. Nonlinear wave propagation and resulting wave height variations are automatically produced as part of the calculation procedure. The unsteady asymmetrical currents and instantaneous water surface variations as solutions to the governing equations are only obtainable with the aid of large, high-speed computers. Solution techniques and applications are in their infancy. Wave breaking and surfzone simulations have yet to be implemented."

At the time of this prediction, Boussinesq models were scarce, difficult and time-consuming to run, and relatively undeveloped for practical physical applications. Very few explicit calculations of coastal wave propagation, and none of surfzone processes, had been made using models based on the Boussinesq theory, and the long term averaging of model results needed to obtain predictions of mean currents had not been performed. The conclusion that the Boussinesq model approach could provide an advantage over the more well established procedure of using a radiation stress field to drive a slowly varying mean current field (see Özkan-Haller and Kirby (1999) for a recent example) was met by occasional skepticism, as evidenced for example by the discussion of Basco's paper by Kirby and Dalrymple (1984).

In the years from 1983 to the present, events have firmly indicated that Basco was correct in his original assessment. Modeling schemes based on Boussinesq equations coupled with innovative

extensions to the theoretical framework have been shown to be accurate and revealing predictors of a wide range of nearshore hydrodynamic behavior, including wave propagation and shoaling, wave current interaction, wave breaking and the generation of nearshore circulation, wave structure interaction and a range of additional topics. The availability of faster computers is bringing the modeling technique into the realm of practical calculations, and model codes have been documented and are, in some cases (Kirby et al (1998), for example) freely available to the public.

This review provides an overview of several aspects of the recent development of the Boussinesq modeling technique, aimed especially at providing a description or predictive capability in the nearshore ocean. The review highlights the work of myself and my colleagues at the University of Delaware over the past decade, and is thus in some sense somewhat narrow in it's orientation. I have attempted to provide balanced indications of the work of other groups in the field, but there will certainly be omissions, and for those I apologize in advance.

The review proceeds by providing an overview of the development of modern fully nonlinear Boussinesq theory in Section 2, and provides several examples illustrating wave shoaling and propagation properties as well as a test of the generation and advection of a vertical-core vortex structure. Section 3 turns to practical extensions to the $O(\mu^2)$ theory, which provides the foundation of most operational Boussinesq models at this time. Extensions to curvilinear coordinates and the inclusion of wave breaking, bottom friction and subgrid-scale mixing are described and illustrated. Section 4 discusses the problem of nearshore circulation, and describes example calculations addressing the generation of longshore currents, longshore current instability and formation of shear waves, and the generation and destabilization of rip currents. Section 5 discusses recent results including vertical shear effects (or the presence of horizontal vorticity). Miscellaneous topics are discussed in Section 6, including the use of Boussinesq models to assist in the depth inversion problem, and an application to tsunami propagation and inundation.

2 Boussinesq Equations for Wave Propagation

The onset of recent developments in the field of Boussinesq models was triggered by two events. The first was the increasing availability of the computer resources needed to run the models. The second was the development of variants of the theory which could be optimized to obtain better dispersion properties at larger kh values, thus allowing the model to treat a larger range of water depths. Critical steps in this process were provided by Madsen, Murray and Sørensen (1991), who established a procedure for optimizing model performance through rearrangement of dispersive terms, and Nwogu (1993), who demonstrated the flexibility obtained by using the horizontal velocity at a given elevation in the water column as a dependent variable. Both procedures have been extensively utilized in the development of subsequent theory. The review articles of Kirby

(1997) and Madsen and Schäffer (1999) and the book by Dingemans (1997) provide extensive reviews of these developments up to 1999, and therefore the material here is concentrated on more recent developments. In addition, the subjects of wave interaction with permeable structures, surf and swash zone sediment transport, and frequency domain modeling are covered elsewhere in this volume and are thus largely neglected here.

2.1 Hydrodynamic fundamentals

Almost all Boussinesq-type models are derived from the framework of incompressible, inviscid flow. (The exception will be the case of waves with horizontal vorticity or vertical shear, considered in section 5) To proceed, a scaling which is appropriate to the regime where wavelength exceeds water depth is chosen.

$$(x,y) = (k_0 x', k_0 y'); z = z'/h_0; t = \sqrt{g h_0 k_0^2}\, t'; \eta = \eta'/a_0; \phi = \left(\frac{a_0\sqrt{g h_0}}{k_0 h_0}\right)^{-1} \phi' \qquad (1)$$

where primes denote dimensional variables, and where h_0 is a depth scale, a_0 is a wave amplitude scale, and k_0 is an inverse horizontal length scale. The dependent variables are surface displacement η and velocity potential ϕ. Velocity components are then given by

$$\mathbf{u} = (u,v) = \nabla\phi \qquad (2)$$

for horizontal velocities, where $\nabla = (\partial/\partial x, \partial/\partial y)$, and

$$w = \phi_z \qquad (3)$$

for vertical velocity, where subscripts x, y, z or t will denote partial derivatives. The resulting scaled problem is characterized by the dimensionless ratios

$$\mu = k_0 h_0; \qquad \delta = a_0/h_0 \qquad (4)$$

The parameter μ characterizes frequency dispersion, and the limit $\mu \to 0$ represents the non-dispersive limit. The designation *weakly dispersive* refers to the regime $\mu \ll 1$. The parameter δ characterizes nonlinearity, and the limit $\delta \to 0$ represents the linear limit. The designation *weakly nonlinear* refers to the regime $\delta \ll 1$. In the present context, we will use the terminology *fully nonlinear* to indicate that no truncation based on powers of δ is employed in obtaining the corresponding model equations. The resulting set of scaled equations is given by

$$\nabla^2\phi + \frac{1}{\mu^2}\phi_{zz} = 0, \qquad -h \le z \le \delta\eta \qquad (5)$$

$$\nabla h \cdot \nabla\phi + \frac{1}{\mu^2}\phi_z = 0, \qquad z = -h \qquad (6)$$

$$\eta + \phi_t + \frac{\delta}{2}\left(|\nabla\phi|^2 + \frac{1}{\mu^2}(\phi_z)^2\right) = 0, \qquad z = \delta\eta \qquad (7)$$

$$\eta_t + \delta\nabla\eta\cdot\nabla\phi - \frac{1}{\mu^2}\phi_z = 0, \qquad z = \delta\eta \qquad (8)$$

Equation (8) is often replaced by a depth integrated form of (5) which uses (6) and (8) to resolve boundary terms, giving

$$\eta_t + \nabla \cdot \mathbf{M} = 0; \qquad \mathbf{M} = \int_{-h}^{\delta\eta} \nabla\phi dz \tag{9}$$

The central feature of Boussinesq wave theories is that the solution to (5) - (6) is usually given as a power series in z, after which the surface boundary conditions are employed to obtain evolution equations. The choice of a reference elevation for the series expansion in z is initially fairly arbitrary. Following Madsen and Schäffer (1998), an expansion about the still water level of the form

$$\phi(x, y, z, t) = \sum_{n=0}^{\infty} z^n \phi^{(n)}(x, y, t) \tag{10}$$

gives, after substitution in (5),

$$\phi(x, y, z, t) = \sum_{n=0}^{\infty} (-1)^n \mu^{2n} \left(\frac{z^{2n}}{(2n)!} \nabla^{2n} \phi^{(0)} + \frac{z^{2n+1}}{(2n+1)!} \nabla^{2n} \phi^{(1)} \right) \tag{11}$$

where $\phi^{(0)}$ and $\phi^{(1)}$ represent ϕ and ϕ_z evaluated at $z = 0$ and are unknown prior to applying boundary conditions. Agnon et al (1999) demonstrate that (11) recovers the full linear solution for a slowly varying plane wave over a mild bottom slope.

The standard procedure for developing Boussinesq models follows from using the bottom boundary condition (6) to eliminate the $\phi^{(1)}$ unknown in favor of $\phi^{(0)}$ (or a suitably defined replacement), after which the development proceeds using a truncated expansion for ϕ. We concentrate on this procedure below. More recently, Agnon et al (1999) and Madsen et al (2002) have pursued a path where the identity of horizontal and vertical velocities is maintained through much of the derivation, adding a dependent variable but increasing flexibility in optimizing results. This procedure will be discussed in section 2.4.

2.2 The weakly dispersive problem

The full linear problem taken from (5) - (8) describes propagating water waves with a dispersion relation given by

$$\omega^2 = gk \tanh kh \tag{12}$$

or, equivalently,

$$c^2 = gh \frac{\tanh kh}{kh} \tag{13}$$

where ω denotes angular frequency, k denotes magnitude of a wavenumber vector $\mathbf{k}$, and c denotes phase speed for a monochromatic wave component. In the limit $\mu \ll 1$, the ratio in (13) should approach 1, and hence $c^2 \sim gh$. The resulting waves are nearly nondispersive, with a leading order correction of the form

$$c^2 = gh(1 + O(kh)^2) \tag{14}$$

Obviously, an approximation of this form can impose severe restrictions when the problem of propagating water waves in a general domain with a range of water depths is considered. In modern terms, the principle goal of most derivations of Boussinesq models is to obtain an approximation to the ratio in (13) which is fairly robust over a range of values of kh; i.e., extending outside of the limit $\mu \to 0$.

Following Nwogu (1993), we define a reference elevation z_α located within the water column, and re-express the series expansion for ϕ in terms of the value at z_α. Using the bottom boundary condition (6) and truncating the resulting series after $O(\mu^2)$ gives

$$\phi(x,y,z,t) = \phi_\alpha(x,y,t) + \mu^2(z_\alpha - z)\nabla\cdot(h\nabla\phi_\alpha) - \frac{1}{2}\mu^2({z_\alpha}^2 - z^2)\nabla^2\phi_\alpha + O(\mu^4) \qquad (15)$$

Substituting (15) in linearized versions of (7) and (9) (with $\delta = 0$) and using $\phi_\alpha \sim \exp i(kx - \omega t)$ gives the dispersion relation

$$\omega^2 = gk^2h\frac{1 - (\alpha + 1/3)(kh)^2}{1 - \alpha(kh)^2} \qquad (16)$$

where

$$\alpha = \frac{1}{2}\left(\frac{z_\alpha}{h}\right)^2 + \frac{z_\alpha}{h} \qquad (17)$$

The choice of α fixes the resulting dispersion relation and the corresponding value of z_α. $\alpha = -1/3$ reproduces the classical Boussinesq theory based on depth-averaged velocity, while the choice $\alpha = -2/5$ reproduces the $(2,2)$ Padé approximant to (13). Nwogu further adjusted the second result by choosing α to minimize a measure of phase speed error over a range of kh values, and obtained $\alpha = -0.39$. A comparison of the true linear dispersion relation (13) and the approximate form (16) is shown in Figure 1, and shows that reasonably accurate dispersion can be obtained for a range of μ values up to about 3. The next order of approximation is discussed in section 2.4.

2.3 Weak vs. full nonlinearity in the $O(\mu^2)$ Boussinesq formulation

Subsequent to the initial work on improved linear dispersion, the next topic to draw attention was the problem of relaxing the restriction of weak nonlinearity in the problem formulation. The need for this extension is clear when one realizes that the wave height to water depth ratio essentially is of $O(1)$ in the surfzone and just seaward of it. The most obvious line of approach staying within the Boussinesq type of formulation is to drop the notion of pursuing an expansion in powers of δ, and instead use the weakly dispersive expression for ϕ or horizontal velocity $\mathbf{u}$ in the form of a power series in μ^2 to evaluate the complete surface boundary condition. We will subsequently refer to models resulting from this procedure as *fully nonlinear models*, in the sense that all of the available information on velocities is used to evaluate the full boundary conditions. Numerous early examples of this approach appear in the literature and have been reviewed by Dingemans (1997), Kirby (1997) and Madsen and Schäffer (1999). We restrict our attention here to two examples; those

of Wei et al (1995) and Liu (1994). Following the procedure of Nwogu (1993), each study derived a set of model equations for potential flow written initially in terms of ϕ_α and η given by the volume conservation equation (9) and the Bernoulli equation (7). Using expression (15) in (9) and (7) gives

$$\begin{aligned}\mathbf{M} &= H\left[\nabla\phi_\alpha+\mu^2\left\{\nabla\left[z_\alpha\nabla\cdot(h\nabla\phi_\alpha)+\frac{{z_\alpha}^2}{2}\nabla^2\phi_\alpha\right]\right.\right.\\ &\left.\left.+\frac{(h-\delta\eta)}{2}\nabla(\nabla\cdot(h\nabla\phi_\alpha))-\frac{(h^2-h\delta\eta+(\delta\eta)^2)}{6}\nabla^2\nabla\phi_\alpha\right\}\right] \qquad (18)\end{aligned}$$

for volume flux (where $H=h+\delta\eta$ is the total water depth), and

$$\begin{aligned}\eta &+ \phi_{\alpha t}+\frac{\delta}{2}\nabla\phi_\alpha\cdot\nabla\phi_\alpha+\mu^2\left[(z_\alpha-\delta\eta)\nabla\cdot(h\nabla\phi_{\alpha t})+\frac{1}{2}({z_\alpha}^2-(\delta\eta)^2)\nabla^2\phi_{\alpha t}\right]\\ &+ \delta\mu^2\left\{\nabla\phi_\alpha\cdot[\nabla z_\alpha\nabla\cdot(h\nabla\phi_\alpha)+(z_\alpha-\delta\eta)\nabla(\nabla\cdot(h\nabla\phi_\alpha))]\right\}\\ &+ \delta\mu^2\left\{\nabla\phi_\alpha\cdot\left[z_\alpha\nabla z_\alpha\nabla^2\phi_\alpha+\frac{1}{2}({z_\alpha}^2-(\delta\eta)^2)\nabla(\nabla^2\phi_\alpha)\right]\right\}\\ &+ \delta\mu^2\left\{\frac{1}{2}[\nabla\cdot(h\nabla\phi_\alpha)]^2+\delta\eta\nabla\cdot(h\nabla\phi_\alpha)\nabla^2\phi_\alpha+\frac{1}{2}(\delta\eta)^2(\nabla^2\phi_\alpha)^2\right\}=0 \qquad (19)\end{aligned}$$

for the Bernoulli equation. These results were found independently by Liu (1994) and Wei et al (1995).

An alternate model in terms of η and horizontal velocity $\mathbf{u}_\alpha$ at the reference level z_α is preferred for practical use, as it is extendable to include breaking, frictional and mixing effects. Substituting for $\nabla\phi_\alpha$ in (18) using

$$\nabla\phi_\alpha=\mathbf{u}_\alpha-\mu^2[\nabla z_\alpha\nabla\cdot(h\mathbf{u}_\alpha)+z_\alpha\nabla z_\alpha\nabla\cdot\mathbf{u}_\alpha]+O(\mu^4) \qquad (20)$$

gives

$$\begin{aligned}\mathbf{M} &= H\left[\mathbf{u}_\alpha+\mu^2\left\{\left[\frac{1}{2}{z_\alpha}^2-\frac{1}{6}(h^2-h\delta\eta+(\delta\eta)^2)\right]\nabla(\nabla\cdot\mathbf{u}_\alpha)\right.\right.\\ &\left.\left.+\left[z_\alpha+\frac{1}{2}(h-\delta\eta)\right]\nabla(\nabla\cdot(h\mathbf{u}_\alpha))\right\}\right]+O(\mu^4) \qquad (21)\end{aligned}$$

for volume flux. Taking the horizontal gradient of (19) leads to a horizontal momentum equation which may be written schematically in the form

$$\mathbf{u}_{\alpha t}+\delta(\mathbf{u}_\alpha\cdot\nabla)\mathbf{u}_\alpha+\nabla\eta+\mu^2\mathbf{V_1}+\delta\mu^2\mathbf{V_2}=O(\mu^4) \qquad (22)$$

In deriving their version of the model equation, Wei et al (1995) erroneously made the substitution

$$\frac{\delta}{2}\nabla(\mathbf{u}_\alpha\cdot\mathbf{u}_\alpha)\rightarrow\delta(\mathbf{u}_\alpha\cdot\nabla)\mathbf{u}_\alpha \qquad (23)$$

after using (20) in the Bernoulli equation. The substitution (23) implies the incorporation of a vorticity term $\boldsymbol{\omega}\times\mathbf{u}_\alpha$, but, as will be shown below, the $O(\mu^2)$ contribution to $\boldsymbol{\omega}$ is missed in this

substitution, as pointed out by Chen et al (2000b) and Hsaio et al (2002). Wei et al (1995) obtained the dispersive terms

$$\begin{aligned}
\mathbf{V_1} &= \frac{1}{2}{z_\alpha}^2\nabla(\nabla\cdot\mathbf{u}_{\alpha t}) + z_\alpha\nabla(\nabla\cdot(h\mathbf{u}_{\alpha t})) - \nabla\left[\frac{1}{2}(\delta\eta)^2\nabla\cdot\mathbf{u}_{\alpha t} + \delta\eta\nabla\cdot(h\mathbf{u}_{\alpha t})\right] \qquad (24)\\
\mathbf{V_2} &= \mathbf{V_{2W}} = \nabla\left[(z_\alpha-\delta\eta)(\mathbf{u}_\alpha\cdot\nabla)(\nabla\cdot(h\mathbf{u}_\alpha)) + \frac{1}{2}({z_\alpha}^2-(\delta\eta)^2)(\mathbf{u}_\alpha\cdot\nabla)(\nabla\cdot\mathbf{u}_\alpha)\right]\\
&\quad +\frac{1}{2}\nabla\left[(\nabla\cdot(h\mathbf{u}_\alpha)+\delta\eta\nabla\cdot\mathbf{u}_\alpha)^2\right] \qquad (25)
\end{aligned}$$

where the $\mathbf{W}$ subscript in $\mathbf{V_{2W}}$ denotes the Wei et al version. In contrast, Liu (1994; see corrected versions in Lynett, Wu and Liu, 2002) invoked the substitution

$$\frac{\delta}{2}\nabla(\nabla\phi_\alpha\cdot\nabla\phi_\alpha) = \delta(\nabla\phi_\alpha\cdot\nabla)\nabla\phi_\alpha \qquad (26)$$

within the original gradient of the Bernoulli equation, and obtained the expression $\mathbf{V_1}$ as in (24). After some rearrangement to get a form close to the Wei et al form $\mathbf{V_{2W}}$, which is a pure gradient, Liu's $\mathbf{V_2}$ may be written as

$$\mathbf{V_{2L}} = \mathbf{V_{2W}} + \mathbf{V_{2r}} \qquad (27)$$

where

$$\begin{aligned}
\mathbf{V_{2r}} &= (\mathbf{u}_\alpha\cdot\nabla z_\alpha)\left[z_\alpha\nabla(\nabla\cdot\mathbf{u}_\alpha)+\nabla(\nabla\cdot(h\mathbf{u}_\alpha))\right]\\
&\quad -\nabla z_\alpha(\mathbf{u}_\alpha\cdot\nabla)(\nabla\cdot(h\mathbf{u}_\alpha)) - z_\alpha\nabla z_\alpha(\mathbf{u}_\alpha\cdot\nabla)(\nabla\cdot\mathbf{u}_\alpha) \qquad (28)
\end{aligned}$$

The physical interpretation of this extra term was discovered by Chen et al (2000b). After some manipulation, $\mathbf{V_{2r}}$ may be written in the compact form

$$\mathbf{V_{2r}} = \boldsymbol{\omega_1}\times\mathbf{u}_\alpha \qquad (29)$$

where $\boldsymbol{\omega_1}$ denotes the $O(\mu^2)$ contribution to vertical vorticity, given by

$$\begin{aligned}
\boldsymbol{\omega_1} &= \mathbf{i_z}\left[z_{\alpha,x}\left[(\nabla\cdot(h\mathbf{u}_\alpha))_{,y}+z_\alpha(\nabla\cdot\mathbf{u}_\alpha)_{,y}\right] - z_{\alpha,y}\left[(\nabla\cdot(h\mathbf{u}_\alpha))_{,x}+z_\alpha(\nabla\cdot\mathbf{u}_\alpha)_{,x}\right]\right]\\
&= \nabla z_\alpha\times\nabla[\nabla\cdot(h\mathbf{u}_\alpha)+z_\alpha\nabla\cdot\mathbf{u}_\alpha] \qquad (30)
\end{aligned}$$

Adding $\mathbf{V_{2r}}$ to the expression (25) corrects the original model of Wei et al (1995). We will refer to the combined set of terms simply as $\mathbf{V_2}$ subsequently. Note that the correction term does not appear in weakly-nonlinear formulations, where terms of $O(\delta\mu^2)$, and hence all of $\mathbf{V_2}$, are neglected. The term also vanishes in water of constant depth, where z_α is constant.

Wei and Kirby (1995) have described a numerical scheme for equations of this type which has come into fairly wide usage. Time stepping is treated using a fourth-order Adams-Bashforth-Moulton scheme, while spatial differencing is handled using a mixed-order scheme, employing fourth-order accurate centered differences for first derivatives and second-order accurate derivatives

for third derivatives. The latter choice is made in order to move leading truncation errors to one order higher than the $O(\mu^2)$ dispersive terms, while maintaining the tridiagonal structure of spatial derivatives within time-derivative terms. Wei and Kirby (1995) used a non-staggered grid scheme with $\mathbf{u}_\alpha$ and η defined at the same locations. More recently, Shi et al (2001a) have used a staggered grid approach which has less apparent sensitivity to treatment of boundary conditions. The staggered grid scheme has become our preferred approach. Methods for generating waves at internal sources have been described by Wei et al (1999) and Chawla and Kirby (2000). Kirby et al (1998) document a version of the non-staggered code, known as *FUNWAVE*, which is available at http://chinacat.coastal.udel.edu/~kirby/programs/funwave.

Properties of this model for wave propagation problems have been reviewed by Kirby (1997) and Madsen and Schäffer (1999). The ability of the model to provide an accurate representation of the evolution and transport of the vertical vorticity component was tested recently by Hommel et al (2000), who compared model results to laboratory data for the case of a vertical vortex core shed during the passage of a solitary wave past a vertical plane wall blocking half the width of a wave flume. These tests were partially motivated by a previous study by Roddier and Ertekin (1999), who had considered the diffraction of a solitary wave at the tip of a breakwater using a potential flow model analogous to the Bernoulli equation formulation (19). Roddier and Ertekin indicated the formation of a deep depression at the breakwater tip, which they explained to be a "bathtub vortex". However, a consideration of their geometry shows that a vortex core could not be forming at a position attached to the tip of the wall, since the presence of the wall would interupt the circulation of fluid around the depression. The depression is simply the manifestation of a singularity in the solution at the breakwater tip, caused by the approach to infinite acceleration as fluid turns the 180° corner. This result shows conclusively that the truly irrotational models in the form of a Bernoulli equation will not spontaneously generate a vortex due to flow separation or advect the vortex away from the generation region. Hommel et al considered the somewhat different case of a breakwater oriented parallel to the crest of the approaching solitary wave. Figure 2 shows a photograph of a vortex core shed during passage of a solitary wave from the left, with the core rotation in the clockwise direction. Figure 3 shows the corresponding numerical result, with velocity vectors overlying a colormap of the vorticity field. In general, agreement between modeled and measured velocity time series were good for these cases. Results are omitted here, and the reader is referred to Hommel et al (2000).

2.4 Extensions to higher order

The $O(\mu^2)$ model described above has provided a robust framework for predicting wave propagation in shallow to intermediate water depths, but still exhibits limitations in predicting water particle kinematics. In particular, predictions of wave-induced horizontal velocity near the seabed breaks

down for values of μ far smaller than implied by the limitations on model dispersion accuracy. For example, the horizontal velocity predicted by the model of Wei et al (1995) falls to zero at $\mu = \sqrt{10}$ and becomes negative in sign (relative to the surface velocity) in deeper water, as illustrated in Figure 4. This type of result renders the $O(\mu^2)$ models useless for prediction of near-bed kinematics (as would be needed in sediment transport calculations) at water depths far smaller than implied by the accuracy of the dispersion relation, unless an artificial means is employed to estimate near-bed velocities from surface values. As a result, the development of higher order approximations in the Boussinesq model has proceeded with the intent both of increasing the range of allowed water depths and with improving the accuracy of kinematic predictions within the allowed range of depths. Two avenues of approach are reviewed here.

2.4.1 Model of Gobbi et al (2000)

One avenue of approach is to retain higher order terms in the expansion for ϕ, and then proceed in constructing either the two-equation model in η, ϕ^* or the three-equation model in $\eta, \mathbf{u}^*$, where superscript $*$ indicates a particular choice of reference level or combination of reference levels used to specify the value of the potential or horizontal velocity. This procedure poses difficulties right away, as the method proposed by Nwogu (1993) does not provide access to higher-order versions of the Padé form of the dispersion relation (Dingemans, 1997). For example, at $O(\mu^4)$ in the expansion for ϕ, the desired expansion of the usual dispersion relation is given by

$$\frac{\tanh \mu}{\mu} = \frac{1 + (1/9)\mu^2 + (1/945)\mu^4}{1 + (4/9)\mu^2 + (1/63)\mu^4} + O(\mu^{10}) \tag{31}$$

The resulting phase speed estimate is shown in Figure 1. Gobbi et al (2000) approached this problem by constructing a potential formulated as the weighted average of the potential at two Nwogu-type reference levels,

$$\tilde{\phi} = \beta \phi_a + (1 - \beta)\phi_b \tag{32}$$

where ϕ_a and ϕ_b are defined as in the previous section and are evaluated at levels z_a and z_b. Relationships between these parameters giving the appropriate dispersion relationship are given by (Gobbi et al, 2000)

$$z_a = \left[\frac{1}{9} - \left\{\frac{8\beta}{567(1-\beta)}\right\}^{1/2} + \left\{\frac{8}{567\beta(1-\beta)}\right\}^{1/2}\right]^{1/2} - 1, \tag{33}$$

$$z_b = \left[\frac{1}{9} - \left\{\frac{8\beta}{567(1-\beta)}\right\}^{1/2}\right]^{1/2} - 1, \tag{34}$$

Values $0.018 < \beta < 0.467$ give z_a and z_b levels lying within the water column and recover the form (31). The resulting truncated potential is given by

$$\begin{aligned} \phi &= \tilde{\phi} + \mu^2 \left[(Ah - \zeta) F_1(\tilde{\phi}) + \left(Bh^2 - \zeta^2\right) F_2(\tilde{\phi})\right] + \mu^4 \left[(Ah - \zeta) F_3(\tilde{\phi})\right. \\ &+ \left.\left(Bh^2 - \zeta^2\right) F_4(\tilde{\phi}) + \left(Ch^3 - \zeta^3\right) F_5(\tilde{\phi}) + \left(Dh^4 - \zeta^4\right) F_6(\tilde{\phi})\right], \end{aligned} \tag{35}$$

where $\zeta = h + z$, and where

$$A \equiv \frac{1}{h}\left[\beta(h+z_a) + (1-\beta)(h+z_b)\right], \tag{36}$$

$$B \equiv \frac{1}{h^2}\left[\beta(h+z_a)^2 + (1-\beta)(h+z_b)^2\right], \tag{37}$$

$$C \equiv \frac{1}{h^3}\left[\beta(h+z_a)^3 + (1-\beta)(h+z_b)^3\right], \tag{38}$$

$$D \equiv \frac{1}{h^4}\left[\beta(h+z_a)^4 + (1-\beta)(h+z_b)^4\right], \tag{39}$$

and

$$F_1(\tilde{\phi}) \equiv G\nabla h \cdot \nabla\tilde{\phi}, \tag{40}$$

$$F_2(\tilde{\phi}) \equiv \frac{1}{2}G\nabla^2\tilde{\phi}, \tag{41}$$

$$F_3(\tilde{\phi}) \equiv \nabla h \cdot \nabla\left(Ah\nabla h \cdot \nabla\tilde{\phi}\right) + \frac{1}{2}\nabla h \cdot \nabla\left(Bh^2\nabla^2\tilde{\phi}\right), \tag{42}$$

$$\begin{aligned} F_4(\tilde{\phi}) &\equiv \frac{1}{2}\nabla^2\left(Ah\nabla h \cdot \nabla\tilde{\phi}\right) + \frac{1}{4}\nabla^2\left(Bh^2\nabla^2\tilde{\phi}\right) \\ &- \frac{1}{2}^2\nabla^2 h\nabla h \cdot \nabla\tilde{\phi} - \nabla h \cdot \nabla\left(\nabla h \cdot \nabla\tilde{\phi}\right), \end{aligned} \tag{43}$$

$$F_5(\tilde{\phi}) \equiv -\frac{1}{6}\nabla^2 h\nabla^2\tilde{\phi} - \frac{1}{3}\nabla h \cdot \nabla\left(\nabla^2\tilde{\phi}\right) - \frac{1}{6}\nabla^2\left(\nabla h \cdot \nabla\tilde{\phi}\right), \tag{44}$$

$$F_6(\tilde{\phi}) \equiv -\frac{1}{24}\nabla^2\left(\nabla^2\tilde{\phi}\right). \tag{45}$$

where $G = (1 + \mu^2|\nabla h|^2)^{-1}$. Seeking a model system in terms of a horizontal velocity, Gobbi and Kirby (1999) introduced the definition

$$\tilde{\mathbf{u}}(x,y,t) = \beta\left[\nabla\phi\right]_{z=z_a} + (1-\beta)\left[\nabla\phi\right]_{z=z_b}. \tag{46}$$

where the relationship between $\tilde{\mathbf{u}}$ and $\tilde{\phi}$ is given by

$$\begin{aligned} \nabla\tilde{\phi} &= \tilde{\mathbf{u}} - \mu^2\nabla h\left[(A-1)F_{21} + 2(B-A)hF_{22}\right] \\ &- \mu^4\nabla h\left[(A-1)(F_{41}+F_{43}) + 2(B-A)h(F_{42}+F_{44})\right. \\ &+ \left.3(C-B)h^2F_{45} + 4(D-C)h^3F_{46}\right], \end{aligned} \tag{47}$$

where

$$F_{21}(\tilde{\mathbf{u}}) \equiv G\nabla h \cdot \tilde{\mathbf{u}}, \tag{48}$$

$$F_{22}(\tilde{\mathbf{u}}) \equiv \frac{1}{2}G\nabla \cdot \tilde{\mathbf{u}}, \tag{49}$$

$$F_{41}(\tilde{\mathbf{u}}) \equiv -|\nabla h|^2\left[(A-1)\nabla h \cdot \tilde{\mathbf{u}} + (B-A)h\nabla \cdot \tilde{\mathbf{u}}\right], \tag{50}$$

$$F_{42}(\tilde{\mathbf{u}}) \equiv -\frac{1}{2}\nabla \cdot \left\{\nabla h\left[(A-1)\nabla h \cdot \tilde{\mathbf{u}} + (B-A)h\nabla \cdot \tilde{\mathbf{u}}\right]\right\}, \tag{51}$$

$$F_{43}(\tilde{\mathbf{u}}) \equiv \nabla h \cdot \nabla\left(Ah\nabla h \cdot \tilde{\mathbf{u}}\right) + \frac{1}{2}\nabla h \cdot \nabla\left(Bh^2\nabla \cdot \tilde{\mathbf{u}}\right), \tag{52}$$

$$
\begin{aligned}
F_{44}(\tilde{\mathbf{u}}) &\equiv \frac{1}{2}\nabla^2\left(Ah\nabla h\cdot\tilde{\mathbf{u}}\right)+\frac{1}{4}\nabla^2\left(Bh^2\nabla\cdot\tilde{\mathbf{u}}\right)\\
&- \frac{1}{2}\nabla^2 h\nabla h\cdot\tilde{\mathbf{u}}-\nabla h\cdot\nabla\left(\nabla h\cdot\tilde{\mathbf{u}}\right), \qquad (53)\\
F_{45}(\tilde{\mathbf{u}}) &\equiv -\frac{1}{6}\nabla^2 h\nabla\cdot\tilde{\mathbf{u}}-\frac{1}{3}\nabla h\cdot\nabla\left(\nabla\cdot\tilde{\mathbf{u}}\right)-\frac{1}{6}\nabla^2\left(\nabla h\cdot\tilde{\mathbf{u}}\right), \qquad (54)\\
F_{46}(\tilde{\mathbf{u}}) &\equiv -\frac{1}{24}\nabla^2\left(\nabla\cdot\tilde{\mathbf{u}}\right). \qquad (55)
\end{aligned}
$$

The volume flux $\mathbf{M}$ in (9) is then given by

$$
\begin{aligned}
\mathbf{M} &= H\left\{\tilde{\mathbf{u}}+\mu^2\left[\left(Ah-\frac{H}{2}\right)\left(2\nabla hF_{22}+\nabla F_{21}\right)+\left(Bh^2-\frac{H^2}{3}\right)\nabla F_{22}\right]\right.\\
&+ \mu^4\left[\left(Ah-\frac{H}{2}\right)\left(2\nabla hF_{42}+\nabla F_{41}+2\nabla hF_{44}+\nabla F_{43}\right)\right.\\
&+ \left(Bh^2-\frac{H^2}{3}\right)\left(\nabla F_{42}+3\nabla hF_{45}+\nabla F_{44}\right)\\
&+ \left.\left.\left(Ch^3-\frac{H^3}{4}\right)\left(4\nabla hF_{46}+\nabla F_{45}\right)+\left(Dh^4-\frac{H^4}{5}\right)\nabla F_{46}\right]\right\}, \qquad (56)
\end{aligned}
$$

where $H=h+\delta\eta$ denotes total water depth. The momentum equation may be written as

$$
\mathbf{U}_t=-\nabla\eta-\frac{\delta}{2}\nabla\left(|\tilde{\mathbf{u}}|^2\right)+\Gamma_1\left(\eta,\tilde{\mathbf{u}}_t\right)+\Gamma_2\left(\eta,\tilde{\mathbf{u}}\right), \qquad (57)
$$

where

$$
\begin{aligned}
\mathbf{U} &\equiv \tilde{\mathbf{u}}+\mu^2\left[\left(A-1\right)h\left(2\nabla hF_{22}+\nabla F_{21}\right)+\left(B-1\right)h^2\nabla F_{22}\right]\\
&+ \mu^4\left[\left(A-1\right)h\left(2\nabla hF_{42}+\nabla F_{41}+2\nabla hF_{44}+\nabla F_{43}\right)\right.\\
&+ \left(B-1\right)h^2\left(\nabla F_{42}+3\nabla hF_{45}+\nabla F_{44}\right)\\
&+ \left.\left(C-1\right)h^3\left(4\nabla hF_{46}+\nabla F_{45}\right)+\left(D-1\right)h^4\nabla F_{46}\right], \qquad (58)\\
\Gamma_1 &\equiv \mu^2\nabla\left[\delta\eta F_{21t}+\left(2h\delta\eta+\delta^2\eta^2\right)F_{22t}\right]\\
&+ \mu^4\nabla\left[\delta\eta\left(F_{41t}+F_{43t}\right)+\left(2h\delta\eta+\delta^2\eta^2\right)\left(F_{42t}+F_{44t}\right)\right.\\
&+ \left(3h^2\delta\eta+3h\delta^2\eta^2+\delta^3\eta^3\right)F_{45t}\\
&+ \left.\left(4h^3\delta\eta+6h^2\delta^2\eta^2+4h\delta^3\eta^3+\delta^4\eta^4\right)F_{46t}\right], \qquad (59)\\
\Gamma_2 &\equiv -\mu^2\delta\nabla\left\{\tilde{\mathbf{u}}\cdot\left[\left(Ah-H\right)\left(\nabla F_{21}+2\nabla hF_{22}\right)+\left(Bh^2-H^2\right)\nabla F_{22}\right]\right.\\
&+ \left.\frac{1}{2}\left(F_{21}+2HF_{22}\right)^2\right\}\\
&- \mu^4\delta\nabla\left\{\tilde{\mathbf{u}}\cdot\left[\left(Ah-H\right)\left(\nabla F_{41}+2\nabla hF_{42}+\nabla F_{43}+2\nabla hF_{44}\right)\right.\right.\\
&+ \left(Bh^2-H^2\right)\left(\nabla F_{42}+\nabla F_{44}+3\nabla hF_{45}\right)\\
&+ \left.\left(Ch^3-H^3\right)\left(\nabla F_{45}+4\nabla hF_{46}\right)+\left(Dh^4-H^4\right)\nabla F_{46}\right]\\
&+ \left.\frac{1}{2}\left|\left(Ah-H\right)\right)\left(\nabla F_{21}+2\nabla hF_{22}\right)+\left(Bh^2-H^2\right)\nabla F_{42}\right|^2
\end{aligned}
$$

$$+ \quad \frac{1}{2}\left[\left(F_{21}+2HF_{22}\right)\left(F_{41}+2HF_{42}\right.\right.$$
$$+ \quad \left.\left.F_{43}+2HF_{44}+3H^2F_{45}+4H^3F_{46}\right)\right]\Big\}. \tag{60}$$

Note that (57) retains the form of the Bernoulli term and thus is only applicable to irrotational motion. Uses of the model by Gobbi and Kirby (1999) were limited to one horizontal dimension, and thus no vertical vorticity is generated in any existing results.

The extension to $O(\mu^4)$ of the vertical structure of ϕ in the Gobbi et al model provides a dramatic enhancement of the prediction of velocity components. For example, Figure 4 shows a comparison of vertical profiles of horizontal velocity for the linear, periodic wave case. The prediction is fairly robust up to $\mu = 5$, with a spurious flow reversal first occuring at $\mu = 5.54$ at a dimensionless elevation $z = -0.628$. Similar results are obtained for vertical velocities. Improvements are also documented in prediction of second-harmonic amplitudes over the lower order theory. Systematic improvements in leading order amplitude dispersion were not noted, however.

Systematic improvements were also noted in solitary wave properties, including wave height, water particle velocity at crest, and total energy as functions of normalized phase speed. Figure 5 shows plots of a crest speed parameter ω_s given by

$$\omega_s = 1 - (u_c - F_r)^2 \tag{61}$$

where u_c and F_r are horizontal particle velocity at the crest and wave phase speed both normalized by $\sqrt{gh}$. As the particle velocity varies from zero in linear waves to F_r at limiting wave height, ω_s varies from zero to one. Figure 5 shows exact results due to Tanaka (1986), three levels of a Green-Naghdi theory due to Shields and Webster (1988), and results of the $O(\mu^2)$ theory of Wei et al (1995) and the $O(\mu^4)$ theory of Gobbi et al (2000). Results generally indicate that the present theory has accuracy comparable to level 3 Green-Naghdi theory, which has not been applied in realistic computational settings to date.

The most striking improvement in a practical sense is seen in a study of waves propagating from relatively deep water, over the shallow crest of a bar, and back into deep water, as presented originally in Beji and Battjes (1993). The test geometry and location of wave gages is shown in Figure 6. Gobbi and Kirby considered two test cases for periodic wave propagation over the bar crest, using the theory of Gobbi and Kirby and the $O(\mu^2)$ theory of Wei et al (1995). Figures 7 and 8 show results for Case (c), where waves with an initial $\mu = 1.69$ propagate from deeper water, over the shoal, and back into deeper water. Figure 7 shows results for the Gobbi and Kirby model, and indicates that the model is capable of preserving the overall shape of transmitted waves downstream of the bar, which is the most difficult region to obtain good results in. In contrast, Figure 8 shows results obtained using the Wei et al model. In this case, there is clear damage to phase information in the transmitted wave, despite the fact that shoaling from deeper water to the bar crest was modeled

relatively accurately. The accumulation of phase errors beyond the bar crest in the lower order model could be interpreted as being due to dispersion errors in the relatively less accurate model. However, this is not an entirely satisfactory explanation. In order to test this explanation, Gobbi and Kirby constructed a weakly nonlinear ($\delta = O(\mu^2)$) model system by truncating the Gobbi-Kirby model to $O(\mu^4, \delta\mu^2)$. Results from this case show a similar tendency to accumulate phase errors downwave of the shallow bar crest. Clearly, both full nonlinearity and enhanced dispersion effects play a crucial role in the accuracy of solutions in this case.

2.4.2 Model of Agnon et al (1999) and successors

An alternate approach to extending model derivation to higher order and increased accuracy was originally proposed by Agnon et al (1999), with continuing development, for example, in Madsen et al (2002). In this approach, the reduction of the problem to a description in terms of a velocity potential is dropped, and the identity of horizontal velocity $\mathbf{u}$ and vertical velocity w is retained instead. Following Madsen and Schäffer (1998), the irrotational solutions for the velocities may be written as

$$\mathbf{u}(\mathbf{x}, z, t) = \sum_{n=0}^{\infty}(-1)^n \left(\frac{z^{2n}}{(2n)!}\mu^{2n}\nabla(\nabla^{2n-2}(\nabla \cdot \mathbf{u_0})) + \frac{z^{2n+1}}{(2n+1)!}\mu^{2n+2}\nabla(\nabla^{2n}w_0) \right) \tag{62}$$

$$w(\mathbf{x}, z, t) = \sum_{n=0}^{\infty}(-1)^n \left(-\frac{z^{2n+1}}{(2n+1)!}\mu^{2n+2}\nabla^{2n}(\nabla \cdot \mathbf{u_0}) + \frac{z^{2n}}{(2n)!}\mu^{2n+2}\nabla^{2n}w_0 \right) \tag{63}$$

where, following (11),

$$\mathbf{u}_0 = \nabla\phi^{(0)}; \qquad w_0 = \phi^{(1)} \tag{64}$$

are the velocities at $z = 0$. The two velocities are related through the bottom boundary condition (6), giving a relation of the form

$$L_c\{w_0\} + L_s \cdot \{\mathbf{u}_0\} + \nabla h \cdot (L_c\{\mathbf{u}_0\} + L_s\{w_0\}) = 0 \tag{65}$$

where

$$L_c = \sum_{n=0}^{\infty}(-1)^n \frac{h^{2n}}{(2n)!}\nabla^{2n}, \qquad L_s = \sum_{n=0}^{\infty}(-1)^n \frac{h^{2n+1}}{(2n+1)!}\nabla^{2n+1} \tag{66}$$

A great deal of flexibility is left in choosing a procedure for improving the truncated series appearing in (65) during the development of a finite order theory. In Agnon et al (1999), the series form of (65) is multiplied by a differential operator of the form

$$A = 1 + a_2h^2\nabla^2 + a_4h^4\nabla^4 + \cdots \tag{67}$$

and coefficients are then chosen to force terms to dissappear in the resulting equation up to the required order. For example, for constant depth and a truncation level $N = 4$, the resulting equation is

$$(1 - \frac{4}{9}h^2\nabla^2 + \frac{1}{63}h^4\nabla^4)w_0 + (h\nabla - \frac{1}{9}h^3\nabla^3 + \frac{1}{945}h^5\nabla^5) \cdot \mathbf{u}_0 \tag{68}$$

which is correct to $O(\mu^8)$ and reproduces (4,4) Padé dispersion as in Gobbi et al. Agnon et al extend this procedure to include mild slope terms limited to $O(\nabla h)$, possibly limiting the accuracy of the resulting model when applied to abrupt nearshore bathymetry. Once the form of the relation between $\mathbf{u}_0$ and w_0 is obtained, Agnon et al develop expressions for velocities at the free surface in terms of the velocities at $z = 0$, and then employ the evolution equations in terms of $\mathbf{V} = \nabla\Phi$, where $\Phi = \phi(\mathbf{x}, z = \eta, t)$ as in Dommermuth and Yue (1987) and others. Madsen et al (2002) further generalize this procedure by choosing to develop series for the velocities at the arbitrary reference level z_α rather than the still water level $z = 0$. The additional freedom in the system of equations is then utilized to improve the vertical profile of horizontal velocity rather than the dispersion relation, which is already quite accurate.

The line of attack initiated in these studies holds a great deal of promise. In particular, it is much more likely that any access to an actual model system for cases of higher accuracy than that in Gobbi et al would come from this procedure rather than from direct expansion in terms of the velocity potential. Additional publications detailing both theoretical aspects and numerical treatments of the method will be shortly forthcoming.

3 Practical extensions to the $O(\mu^2)$ Boussinesq model

The $O(\mu^2)$ model written in terms of a velocity variable provides an easily extensible framework for the development of a nearshore processes model. In order to achieve this goal, various additional physical processes are incorporated, often on an ad hoc basis. In this section, we consider the extension of the model equation (22) to the form

$$\mathbf{u}_{\alpha t} + \delta(\mathbf{u}_\alpha \cdot \nabla)\mathbf{u}_\alpha + \nabla\eta + \mu^2\mathbf{V_1} + \delta\mu^2\mathbf{V_2} - \mathbf{R_b} - \mathbf{R_s} + \mathbf{R_f} = O(\mu^4) \tag{69}$$

where $\mathbf{R_b}$ denotes wave breaking effects, $\mathbf{R_f}$ denotes bottom friction, and $\mathbf{R_s}$ denotes subgrid-scale lateral mixing effects.

3.1 Improving model dispersion, shoaling and nonlinear properties

As has been shown in a number of studies starting with Madsen et al (1991), improvements in Boussinesq model performance can introduced by employing rearrangements that alter the definitions of $\mathbf{M}$, $\mathbf{V_1}$ and $\mathbf{V_2}$ terms in the model equations, or by redefining the reference configuration of the dependent variables, leading to the same sort of rearrangement. The effectiveness of any modification can be established by examining linear properties such as shoaling and dispersion, along with nonlinear properties such as the amplitudes of harmonics or the magnitude of amplitude dispersion in Stokes wave solutions. We consider two cases in particular.

In order to provide a degree of freedom for use in optimizing nonlinear model properties, Kennedy et al (2001) modified the formulation of Wei et al (1995) by allowing the reference el-

evation z_α to depend on time and thus follow the rise and fall of the local water surface in some manner. The most general case considered defined z_α as

$$z_\alpha = \zeta h + \beta \delta\eta \tag{70}$$

where the original theory of Wei et al is recovered by taking $\beta = 0$ and $\zeta = -1 + \sqrt{1/5}$, corresponding to the (2,2) Padé case. A special case of this relationship occurs when $\beta = \zeta + 1 = \sqrt{1/5}$, which gives

$$z_\alpha = -h + \beta H \tag{71}$$

This case corresponds to choosing a reference level which remains at a fixed proportion of the instantaneous total water depth, and would be equivalent to choosing a fixed σ_α reference level in a $\sigma-$coordinate model. The revision to the model equations is contained entirely within the $\mathbf{V_1}$ term (24), which is revised to read

$$\mathbf{V_1} = \left[\frac{1}{2}{z_\alpha}^2 \nabla(\nabla \cdot \mathbf{u}_\alpha) + z_\alpha \nabla(\nabla \cdot (h\mathbf{u}_\alpha))\right]_t - \nabla\left[\frac{1}{2}(\delta\eta)^2 \nabla \cdot \mathbf{u}_{\alpha t} + \delta\eta \nabla \cdot (h\mathbf{u}_{\alpha t})\right] \tag{72}$$

Kennedy et al examined the optimal choice of β by examining a Stokes wave solution of the form

$$\eta = a_1[\cos(kx - \omega t) + a_+ \cos 2(kx - \omega t) + a_-] \tag{73}$$

where a_+ is a normalized second harmonic amplitude and a_- represents the steady setdown. Forcing the Taylor series expansions of the resulting second harmonic amplitude to match the Taylor series for the second harmonic amplitude of a regular Stokes wave for the full dispersive theory gives the choice $\beta = 17\sqrt{5}/200$. Figure 9 shows plots of the resulting second harmonic amplitudes and setdown, normalized by the correct solutions, for a range of $\mu = kh$ values. The second harmonic amplitude from the optimized model behaves quite well in comparison to the result from the original Wei et al theory, and thus this revision to the original model is highly recommended.

Several studies have examined the enhancement of the $O(\mu^2)$ evolution equations in order to obtain higher-order dispersion. Schäffer and Madsen (1995) applied operators to rearrange dispersive terms in the weakly nonlinear model equations of Nwogu (1993) and obtained four sets of operator coefficients that would recover the more accurate (4,4) Padé dispersion relation in the model system, without adding higher order terms as in the model of Gobbi et al. Madsen and Schäffer (1998) extended this procedure to the fully nonlinear equations of Wei et al (1995). Madsen and Schäffer also demonstrated a procedure for recovering a model expressed entirely in terms of $O(\mu^2)$ terms at the highest, but starting with an $O(\mu^4)$ model and then choosing a form which was expressed only in $O(\mu^2)$ terms by means of operator rearrangements and choice of coefficients. Kennedy et al (2002) have extended this procedure, starting with the $O(\mu^4)$ model of Gobbi and Kirby (1999) in order to retain the very accurate vertical velocity profile given there. Kennedy et al employed two procedures, one based solely on choice of coefficients, and the second based on a combination of

operator rearrangement and choice of coefficients, to obtain model equations expressed in terms of $O(\mu^2)$ terms at the highest. The resulting model retains the (4,4) Padé dispersion of the Gobbi and Kirby model. Following Madsen and Schäffer, Kennedy et al choose the remaining free parameters in order to optimize an integrated shoaling coefficient, which represents a measure of error in local shoaling effects integrated across the entire shoaling zone. Results for this measure are shown in Figure 10 in comparison to results derived from Nwogu's model and from the study of Madsen and Schäffer. The results for the more involved optimization are almost graphically indistinguishable from the exact linear shoaling theory for the vertical resolution chosen in the plot.

3.2 Extensions to non-Cartesian coordinate systems

It is often necessary to apply Boussinesq models in complex geometries. This problem has classically been approached by employing stair-step boundaries in existing Cartesian-grid finite difference codes. Resulting models can be robust, but there is evidence (as discussed below) that such an approach can lead to spurious wave scattering behavior along oblique wall sections. Several more modern approaches have been employed to solve this problem.

The first approach involves switching to a numerical solution method which is not tied to a regular gridding scheme. Finite element techniques are often the principal choice in this approach, and the technique has been extensively developed for application to Boussinesq models. Recent examples include the work of Li et al (1999), Walkley and Berzins (1999), Sørensen and Sørensen (2000) and Woo and Liu (2001).

A second approach is based on employing either analytic or numerically determined coordinate transformations in order to obtain a boundary fitted coordinate system, in which major boundary segments lie along constant values of the fitted coordinates. Methods for obtaining coordinate transformations numerically are well developed in the computational fluid dynamics literature; for example, Shi et al (2001a) employ the scheme of Brackbill and Saltzman (1982) and have developed a publically available Matlab code which may be obtained at http://chinacat.coastal.udel.edu/~kirby/programs/. Several levels of transformation can be employed in such an approach. At the simplest level, the transformation can be applied to the coordinate system only, while the identity of the surface elevation η, x velocity component u and y velocity component v are retained but determined at grid points in the new coordinate system. Results obtained with this approach are perhaps somewhat easier to interpret, but the resulting transformed governing equations are quite cumbersome; see, for example, the discussion of model equations in Li and Zhan (2001).

A more involved approach involves defining a tensor transformation applied to the velocity components as well as the coordinate system. Shi et al (2001a,b) employed such an approach, and chose to formulate the resulting model in terms of contravariant velocity components, which are defined to be the velocity components perpendicular to coordinate lines at each point in the

modeled domain. Warsi (1993) provides an extensive discussion of the geometric considerations. While the overhead of learning the details of the metric tensor geometry can be considerable, the approach leads to a much more compact representation of the governing equations than is obtained in a method based on the primitive variables.

Shi et al (2001a,b) provide a number of examples illustrating computations in generalized curvilinear coordinates. Figures 11 and 12 illustrate the propagation of an initially plane wave into a circular channel. The computation in a polar coordinate system corresponds closely to the analytic solution in the linear limit, as shown by Shi et al (2001a). In contrast, a similar calculation in a reasonably finely-resolved Cartesian grid with stair-step boundaries produces a clear excess of scattered wave components in comparison to the polar case.

Shi et al (2001b) have also applied the model to the case of a coastal inlet and have compared model results to measurements of surface elevation, skewness and asymmetry obtained from a laboratory scale model. Detailed model-data comparisons for this case have been completed and are presently under review for publication elsewhere.

3.3 Shoreline conditions

The waterline on a beach subjected to wave action is highly variable, and thus the physical domain in a nearshore Boussinesq model application changes in time. Although it is possible to utilize a time-dependent, shoreline-following grid system in order to resolve the fluid domain only up to the waterline (for example, Özkan-Haller and Kirby, 1997), it is difficult to do so if the shoreline does not remain single valued or becomes multiply connected. For this reason, it is more standard to employ techniques whereby the entire region which is potentially wetted is treated as an active part of the computational grid. One of the earliest methods along this line is the "slot" method of Tao (1984), in which deep, narrow, flooded slots are added to each grid row, extending down at least to the lowest elevation that will be experienced during shoreface rundown. Kennedy et al (2000a) employed the slot technique of Tao but modified it to better enforce mass conservation. The reader is referred there for details. Utilization of slot methods remains something of an art form to date. Slots which are too wide relative to the model grid spacing admit too much fluid before filling during runup, and cause both a reduction in amplitude and a phase lag in modeled runup events. At the other extreme, slots which are too narrow tend to induce a great deal of numerical noise, leading to the need for intermittent or even fairly frequent filtering of swash zone solutions.

Alternately, several moving boundary techniques where the occurance of a shoreline is traced on a fixed grid have been proposed. In one such method, Lynett et al (2002) determine the position of the shoreline on a beach face by linearly extrapolating the surface and velocities from the two wetted grid points closest to shore. Derivatives at wetted grid points are then computed using the regular finite difference stencil including extrapolated values, eliminating the need for conditional

application of off-centered difference stencils near shore. The time stepping solution is then only performed for the wetted grid points. Although this method does not impose any apparent constraints on mass conservation at the shoreline, results for runup of regular and solitary waves are seen to be quite accurate, indicating that the method holds promise for general application.

3.4 Wave breaking

Simulation of wave breaking in Boussinesq models has been approached with a number of techniques, ranging from fairly ad-hoc additions of eddy viscosity formulations up to reasonably detailed calculations of the generation and transport of vorticity or turbulent kinetic energy under the breaking wave crest. Regardless of the formulation, each of the approaches can be thought of as a means for adding the breaking wave force term $\mathbf{R_b}$ to the momentum equation. At minimum, these terms must be scaled similarly in order to reproduce the correct amount of energy dissipation. They must also be localized in the region of the front face of the breaking wave, in order to provide the correct distribution of dissipation in the frequency domain and preserve the proper relative phasing of harmonic components in the wave. Beyond these requirements, the range of physical approaches taken has a great deal of variety.

3.4.1 Eddy viscosity models

Zelt (1991) provided an early model for Boussinesq wave breaking, in the form of an eddy viscosity model applied in a 1-D horizontal model. Extended to 2-D, the breaking wave force term $\mathbf{R_b}$ can be written as

$$R_b^x = \frac{1}{H}\left(\{\nu_b[Hu_\alpha]_x\}_x + \frac{1}{2}\{\nu_b[Hu_\alpha]_y + \nu_b[Hv_\alpha]_x\}_y\right) \tag{74}$$

$$R_b^y = \frac{1}{H}\left(\{\nu_b[Hv_\alpha]_y\}_y + \frac{1}{2}\{\nu_b[Hv_\alpha]_x + \nu_b[Hu_\alpha]_y\}_x\right) \tag{75}$$

Following Zelt, Kennedy et al (2000a) give the breaking wave eddy viscosity as

$$\nu_b = B\delta_b^2 H\eta_t \tag{76}$$

where δ_b is a mixing length coefficient which is calibrated to a value of 1.2. The coefficient B is used to turn the breaking term off or on depending on a criterion based on the vertical velocity of the surface. Again, following Zelt but using time derivatives in place of space derivatives, Kennedy et al used

$$B = \begin{cases} 1, & \eta_t \geq 2\eta_t^* \\ \frac{\eta_t}{\eta_t^*} - 1, & \eta_t^* < \eta_t \leq 2\eta_t^* \\ 0, & \eta_t \leq \eta_t^* \end{cases} \tag{77}$$

The parameter η_t^* determines the onset and cessation of breaking. Zelt chose this criterion to have a constant value, but Kennedy et al use a model for the parameter which involves a time history in

order to allow the slope of the breaking wave crest to relax after the onset of breaking, as in the roller model described below. The relationship is

$$\eta_t^* = \begin{cases} \eta_t^{(F)}, & t \geq T^* \\ \eta_t^{(I)} + \frac{t-t_0}{T^*}(\eta_t^{(F)} - \eta_t^{(I)}), & 0 \leq t - t_0 < T^* \end{cases} \tag{78}$$

Here, T^* is the elapsed time since the onset of the local breaking event, and the initiation and relaxed critical surface velocities are given by $\eta_t^{(I)} = 0.65\sqrt{gh}$ and $\eta_t^{(F)} = 0.15\sqrt{gh}$. In 2-D applications, the relationship must be augmented with a tracking algorithm to follow events along rays; see Chen et al 2000a.

Figure 13 shows an example of bichromatic waves shoaling over a plane beach, including breaking and runup effects. Data is from the laboratory study of Mase (1995). The test verifies the basic features of both the breaking process and the runup using the slot method. Additional two dimensional calculations for wave breaking and runup on a circular island may be found in Chen et al (2000a).

Nwogu and Demirbilek (2001) present a more sophisticated eddy viscosity model in which the eddy viscosity is expressed in terms of turbulent kinetic energy k and a length scale l_t,

$$\nu_b = \sqrt{k} l_t \tag{79}$$

The turbulent kinetic energy is computed using a one-equation model which expresses the generation, horizontal advection, and dissipation of total depth integrated k. Breaking is triggered when horizontal fluid velocity at the surface exceeds the linear estimate of the wave phase speed. Turbulence production falls immediately to zero when this criterion is not exceeded, so there is no relaxation effect as described above or as in the roller model described below.

3.4.2 Roller models

A simplified formulation with a more direct physical interpretation, was developed by Schäffer et al (1993), using the surface roller concept of Svendsen (1984). The model is developed using a two-layer velocity profile, where it is assumed that the velocity u below the elevation of the roller bottom corresponds to the depth-averaged value from irrotational theory, while the roller volume itself is moving at the phase speed c of the wave. The effect of the roller is expressed as a modification to the momentum balance for the organized wave motion. The resulting momentum equation for depth integrated volume flux Q may be written as (in one horizontal dimension)

$$Q_t + \delta \left(\frac{Q^2}{H}\right)_x + gH\eta_x - \mu^2 \frac{h^2}{2} Q_{xxt} + \mu^2 \frac{h^3}{6} \left(\frac{Q}{h}\right)_{xxt} + R_x \tag{80}$$

where R is the excess momentum flux in the roller, given by

$$R = d\left(c - \frac{Q}{H}\right)^2 \left(1 - \frac{d}{H}\right)^{-1} \tag{81}$$

where d is the local roller thickness. Calibration of the model and testing against data are described in Madsen et al (1997), and results are of comparable accuracy to the eddy viscosity models described above.

3.4.3 Vorticity transport models

The most elaborate model of Boussinesq model wave breaking is the vorticity transport model of Veeramony and Svendsen (2000). In this model, there is no a priori separation between roller region and a zone of irrotational flow beneath. Instead, the entire vertical fluid column is treated as a rotational flow, and the vorticity transport equation is solved with simplifying assumptions in order to determine the entire velocity profile over depth. The resulting model is similar to the model of Schäffer et al (1993) in overall form, but the resulting wave breaking terms require more evaluation.

Since the flow is rotational over depth in this treatment, the basic formulation of the problem in terms of a velocity potential is not valid. Veeramony and Svendsen restricted their attention to propagation in one horizontal dimension and formulate the problem in terms of a scalar stream function in the vertical plane,

$$\mu^2 \psi_{xx} + \psi_{zz} = \xi \tag{82}$$

where ψ is the stream function and ξ is the magnitude of the out-of-plane vorticity vector. Boundary conditions are given by

$$\psi(z=-h) = \psi_z(z=-h) = 0 \tag{83}$$

Within the weakly dispersive approximation, (82) may be solved to give

$$\begin{aligned} \psi &= u_0(z+h) - \frac{1}{2}\mu^2(z+h)^2(h_{xx}u_0 + 2h_x u_{0,x}) - \frac{1}{6}\mu^2(z+h)^3 u_{0,xx} \\ &\quad + \int_{-h}^{z}\int_{-h}^{z} \xi dz dz - \mu^2 \int_{-h}^{z}\int_{-h}^{z}\int_{-h}^{z}\int_{-h}^{z} \xi_{xx} dz dz dz dz \end{aligned} \tag{84}$$

where u_0 is the value of the irrotational velocity at the bottom and where terms in u_0 correspond to the usual irrotational theory. In terms of scalar volume flux Q, the resulting Boussinesq momentum equation (without dispersion enhancement) takes on the form

$$Q_t + H\eta_x + \delta\left(\frac{Q^2}{H}\right)_x - \mu^2\frac{h^2}{2}Q_{xxt} + \mu^2\frac{h^3}{6}\left(\frac{Q}{h}\right)_{xxt} + \delta(\Delta M)_x + \mu^2(\Delta P)_{xxt} = 0 \tag{85}$$

Breaking effects are expressed through the quantities ΔM and ΔP, given by

$$\Delta P = \int_{-h}^{\delta\eta}\int_{z}^{\delta\eta}\int_{-h}^{z} (u_r - \overline{u_r}) dz dz dz \tag{86}$$

$$\Delta M = \int_{-h}^{\delta\eta} (u_r^2 - \overline{u_r}^2) dz \tag{87}$$

where $\overline{(*)}$ denotes a depth average. u_r is the rotational component of the horizontal velocity, given by

$$u_r = \int_{-h}^{z} \xi dz - \mu^2 \int_{-h}^{z}\int_{-h}^{z}\int_{-h}^{z} \xi_{xx} dz dz dz + O(\mu^4) \tag{88}$$

The vorticity ξ is formally unknown at this point, and Veeramony and Svendsen (2000) use the leading order terms of the vorticity transport equation, neglecting advective effects to get

$$\xi_t = \kappa \xi_{\sigma\sigma}; \qquad \kappa = \frac{\nu_t}{h^2}; \qquad \sigma = \frac{h+z}{H} \tag{89}$$

Boundary conditions for the vorticity are derived from hydraulic jump experiments described in Svendsen et al (2000). Veeramony and Svendsen solve (89) analytically for the case of eddy viscosity held constant over depth. Figure 14 illustrates the evolution of a vorticity field under a breaking wave crest. Results for undertow profiles were also obtained and show general agreement with laboratory measurements.

Further development of the theory of Veeramony and Svendsen would involve the use of a numerical solution of (89) so that more realistic values of eddy viscosity could be used. However, the extension of the model to two horizontal dimensions is hampered by the use of the stream function formulation, and thus an alternate formulation allowing a three-dimensional flow field is required. The key to this future development may lie in the formulation of Shen (2001), mentioned in Section 5 below.

3.5 Bottom friction and subgrid-scale mixing

Since the velocity field in a Boussinesq calculation resolves the instantaneous wave orbital motion, the choice of a bottom friction formulation is realtively straightforward, and is given in the applications below by

$$\mathbf{R_f} = \frac{f}{H}|\mathbf{u}_\alpha|\mathbf{u}_\alpha \tag{90}$$

where the friction factor is on the order of 10^{-3} in most simulations (Chen et al, 1999, 2000a). Note that the term is written in terms of the reference velocity rather than the bottom velocity, which would tend to reduce the size of f somewhat.

Nearshore current systems are affected by several lateral mixing effects, including both turbulent mixing and lateral shear dispersion resulting from the three-dimensional structure of real currents and their interaction with the wave orbital velocity. Of these, the shear dispersion can be an order of magnitude larger (Svendsen and Putrevu, 1994), and an attempt has been made to incorporate it's effect in most of our nearshore simulations. Chen et al (1999) formulate the effect as a Smagorinsky subgrid model with the form

$$R_s^x = \frac{1}{H}\left(\{\nu_s[Hu_\alpha]_x\}_x + \frac{1}{2}\{\nu_s[Hu_\alpha]_y + \nu_s[Hv_\alpha]_x\}_y\right) \tag{91}$$

$$R_s^y = \frac{1}{H}\left(\{\nu_s[Hv_\alpha]_y\}_y + \frac{1}{2}\{\nu_s[Hv_\alpha]_x + \nu_s[Hu_\alpha]_y\}_x\right) \tag{92}$$

where ν_s is an eddy viscosity arising from the mean flow field,

$$\nu_s = c_m \Delta x \Delta y \left[(U_x)^2 + (V_y)^2 + \frac{1}{2}(U_y + V_x)^2\right]^{1/2} \tag{93}$$

and where U and V are suitable time averages of the velocity field. Chen et al (1999) and subsequent studies have used time averages over two wave periods for regular waves or over ten peak wave periods for irregular waves, and typically use $c_m = 0.25$. This aspect of the model application has not been extensively evaluated. Ongoing work is examining the evolution of shear instabilities in model results as an indicator of the correct level of lateral mixing.

4 Boussinesq Modeling of Nearshore Circulation

Once the effectiveness of breaking and runup models for Boussinesq codes was established, attention rapidly turned to the question of whether the models could provide an accurate rendition of mean currents in the surfzone. A classical analysis of wave-averaged surfzone dyanmics shows that both cross- and longshore mean currents arise due to the presence of gradients of radiation stresses, which represent fluxes of wave-averaged momentum. An analysis of wave-averaged forms of the Boussinesq equations readily shows that the relevant forcing mechanisms are present in the time-dependent form of the evolution equations (Yoon and Liu, 1989), and hence mean currents should be generated in models which account for wave energy dissipation through breaking, which in general would be expressed as $-\rho H \mathbf{u}_\alpha \cdot \mathbf{R_b} + O(\mu^2)$ following from (69). Such a demonstration was provided by Madsen et al (1997). More recently, Peregrine (1998) has examined the instantaneous vorticity dynamics, with particular attention to the idea that vertical vorticity generation in the surfzone is mainly provided by the mechanism

$$\frac{d\omega}{dt} = \nabla \times \mathbf{R_b} \tag{94}$$

where ω is discussed in section 2.3. Peregrine examines the generation of circulation in finite patches of the surfzone and relates it's generation to variations in breaking intensity along wave crests. An example of this mechanism in action is provided in section 4.3 for the case of a rip current stabilized in place by the presence of a channel in a longshore-uniform bar.

4.1 Longshore currents

Chen et al (2000b) have considered the case of longshore current generation in field conditions, using data from the DELILAH field experiment at Duck, North Carolina in October 1990. Figure 15 shows the bathymetry at the experimental site for October 10, 1990. The bar field in this case is nearly longshore uniform aside from a slight kink in bottom contours near the location of an array of crosshore current measurements, indicated by the dashed line. Cross-shore decay of breaking wave heights and resulting longshore currents are indicated by circles in Figure 16(c) and (d), respectively. The longshore current has a strong maximum in the trough between the shoreface and the longshore bar crest, at a location where local forcing due to radiation stress gradients should be weak. Chen et al simulated this experiment using a version of *FUNWAVE* and the wave generation algorithm of

Wei et al (1999) which was extended to cover periodic longshore conditions. A TMA directional wave spectrum was used to provide input conditions (improved simulations using actual measured directional spectra are presently under review for publication). Figure 16 illustrates a snapshot of the surface wave field over the simulated area in panel (a). Refraction of the wave pattern, which is propagating from the lower right, is evident, as is crest splitting in several locations as waves pass over the bar crest. Panel (b) illustrates the time-averaged mean currents in the area. Chen et al show that their is a time-steady net longshore pressure gradient over the stretch of beach in the vicinity of the current measurements, and thus the strong longshore current in the trough is at least partially hydraulically driven. Note that time averaged currents in the Boussinesq model do not reproduce a sufficiently strong undertow, even though the velocity being averaged is located near mid depth. This deficiency is also noted in results of Madsen et al (1997), and occurs because their is no explicit treatment of breaking wave roller volume in the volume conservation equation (9). This deficiency is removed in the 1-D cross-shore model of Veeramony and Svendsen (2000), which recovers undertow values reasonably well, but the correction still remains to be made in most two-dimensional models. Overall, results for longshore currents agree well with data in both laboratory and field settings, providing encouragement that the models are ready to use in realistic settings.

4.2 Shear waves

Based on observations by Oltman-Shay et al (1989), Bowen and Holman (1989) examined the linear stability problem for longshore currents and showed that currents are likely to be unstable for a range of realistic conditions. Özkan-Haller and Kirby (1999) carried out numerical simulations of the same experiment using a radiation stress formulation,and have illustrated the growth to finite amplitude of the instabilities, or *shear waves*. They have shown that the presence of shear waves contributes to the cross-shore mixing that leads to the determination of the longshore current profile, and they have shown that the increase or decrease of imposed dispersive mixing (i.e., the mechanism of Svendsen and Putrevu, 1994) leads to a corresponding decrease or increase in the energetics of the shear wave climate, in such a way that the overall longshore current profile is insensitive to the relative importance of the two mechanisms. This result has not been explained to date, or examined fully in other modeling schemes.

Since shear waves are essentially unsteady motions, it is not immediately clear how to separate them from the incident wave field in a time-domain simulation. Chen et al (1999) approached this problem, in the context of rip currents, by applying a time average over several wave periods in order to suppress the incident wave signature in the modelled velocity field. The resulting filtered velocity field was then differentiated to provide a vertical vorticity field. During this study, Chen et al discovered that a vorticity field constructed directly from the instantaneous horizontal velocities was

similar to the wave-averaged field. In particular, the signature of incident waves in the instantaneous vorticity field is very slight, even after interaction with the underlying vortical current field, and is mainly limited to strong local bottom friction events associated with the passage of wave crests. At the same time, the instantaneous vorticity plots showed more detail in the structure of vortical features such as eddies, since these were not being subjected to an arbitrary low-pass filter.

Figure 17 shows an overlay of a wave-averaged current field and resulting derived vorticity field for the October 10, 1990 DELILAH case described above. For the field cases, the choice of an averaging period is not obvious since the wave field is unsteady in time. Averages here are over a period corresponding to 10 peak wave periods. Vorticity computed from the instantaneous flow field is illustrated in the bottom panel, and shows an energetic flow field associated with growth of instabilities and shedding of eddies to the region offshore of the surfzone (to the right in each panel). Ongoing studies are examining whether these depictions of the flow field are consistant with more detailed array measurements of currents in the field, primarily using data from the Sandyduck experiment in 1997.

4.3 Rip currents

Haller and Dalrymple (2000) performed a laboratory study or a rip current generated on a beach with a fixed channel in an otherwise longshore-uniform bar. The rip was observed to be unstable, leading to lateral motion of the rip both in the rip channel and offshore. An instability analysis provided information on the time scales of fluctuations and the downsteam evolution of mean current profiles which agreed qualitatively with laboratory observations.

Chen et al (1999) examined the experiment of Haller and Dalrymple using the *FUNWAVE* code. The Boussinesq model was shown to reproduce most features of the laboratory experiment, although it was impossible to perform model runs long enough to examine whether the longest time scales observed in the fluctuating laboratory flow field (on the order of 100 seconds) were reproduced in model simulations. Figure 18 illustrates the state of the wave-averaged flow field soon after the initiation of breaking over the bar crest in the simulation. The position of the longshore bar and the rip chennel are outlined by dashed lines in each of the three panels. The middle and lower panel show the presence of strong, localized vorticies fixed at the transition between bar crest and deep rip channel. These are presumably driven at these locations by the mechanism described by Peregrine (1998), and are responsible for the initiation of the rip current jet, which is driven primarily by the dipole forcing provided by the pair of counter-rotating eddies. As the current field evolves further, these vortex pairs are ejected as coherent eddy pairs and advected offshore by the instantaneous jet, after which subsequent eddy pairs form and are also ejected. A portion of such a sequence is illustrated in Figure 19. Figure 20 shows a comparison of long-time averages of cross-shore velocities along 4 longshore transects. The extreme unsteadiness of the rip current leads to a rapid

decay of the time-mean cross-shore velocity offshore of the rip channel. This result is deceptive as a measure of rip strength and must be tempered with the indication of the strength of the instantaneous flow, as indicated in Figure 19.

Overall, Boussinesq models have performed quite well in comparison to both laboratory and field measurements, in situations where flow fields are strongly affected by instability mechanisms and become extremely complex. Further work to examine the energetics of shear wave climates and the mixing of tracers in the cross-shore direction needs to be carried out. In addition, the application of Boussinesq models to the problem of sediment transport and evolution of coastal morphology is underway, and will be a fertile area of work for the next several years.

5 Waves on Vertically Sheared Currents

Waves in coastal regions can be stratified due to the presence of net freshwater runoff, and it is therefore not uncommon to see tidal currents which are sheared over the vertical. The presence of vertical shear greatly complicates the development of appropriate propagation models, since the use of a velocity potential is no longer valid except for the special case of horizontal vorticity components which are uniform over depth (linear current shear).

For the case of propagation in one horizontal dimension, a formulation in terms of a scalar stream function can be employed as in the wave breaking model of Veeramony and Svendsen, describe above. This approach has been explored by Rego et al (2001). Starting with the Poisson equation (82), Rego et al developed a fully nonlinear Boussinesq type equation to $O(\mu^2)$ using a dependent variable $\tilde{u}_\alpha$ defined as the horizontal velocity at reference elevation z_α. For the case of linearized, periodic waves and an imposed current shear, the rather complex model equations yield a dispersion relation given by (in dimensional form)

$$\hat{\omega}^2[1-\alpha(kh)^2] = (gk-\hat{\omega}\gamma_0)kh[1-(\alpha+\frac{1}{3})(kh)^2] + \hat{\omega}k(\gamma_1+k^2\gamma_2) \\ -\hat{\omega}kh\gamma_0[1-\alpha(kh)^2] \tag{95}$$

where the intrinsic frequency is given by

$$\hat{\omega} = \omega - ku_s^c \tag{96}$$

and where ω is absolute frequency, u_s^c is the current velocity at $z=0$,

$$\gamma_0 = \frac{1}{h}\int_{-h}^{0}\xi dz \qquad \gamma_1 = \frac{2}{h}\int_{-h}^{0}\int_{-h}^{z}\xi dz^2 \tag{97}$$

and

$$\gamma_2 = \frac{1}{h}\left\{\int_{-h}^{0}\left[\left((z+h)^2-(z_\alpha+h)^2\right)\int_{-h}^{z}\xi dz\right]dz + \int_{-h}^{0}\int_{z}^{0}\left((z+h)\int_{-h}^{z}\xi dz\right)dz^2\right\} \tag{98}$$

The accuracy of the resulting dispersion relation was checked for several cases by comparing to numerical solutions of the Rayleigh equation following the method of Fenton (1973). Figure 21 shows results for the case of a 1/7 power law profile and a profile given by a cubic polynomial. The results indicate that the model dispersion relation retains accuracy over a range of wavenumbers comparable to the (2,2) Padé dispersion relation for the no-current (or uniform over depth current) case.

As with the wave breaking model of Veeramony and Svendsen (2000), the use of the scalar stream function in the present case makes a general extension to two horizontal dimensions difficult. A way around this can be seen by noting that the derivative of (82) with respect to x gives

$$\mu^2 w_{xx} + w_{zz} = \xi_x \tag{99}$$

giving a problem formulated in terms of vertical velocity w. Starting from the general three-dimensional Euler equations, it is straightforward to show that this relation is generalized by

$$\mu^2 \nabla^2 w + w_{zz} = \nabla \cdot \boldsymbol{\xi} \tag{100}$$

where $\boldsymbol{\xi}$ is now a vector formed by the two horizontal components of the general 3-D vorticity vector. Shen (2001) has explored the use of (100) as a starting point for deriving Boussinesq model equations.

6 Miscellaneous Applications

6.1 Depth inversion

The question of whether the spatial pattern of water depths in the surfzone can be deduced from images of the water surface has been with us since the early days of military amphibious operations. Recently, several successful video-based techniques have been described for waves in slowly varying depth in open water (Dugan et al, 2001) or in the surfzone (Stockdon and Holman, 2000). Each of these methods depends on having dense spatial information and long time series so that both frequency and wavenumber content of the signal can be determined. The direct need for a model-based simulation is then avoided by using the linear wave dispersion relation to relate frequency to wavenumber in order to determine the unknown water depth. Methods of this type are not readily applicable to data streams obtained during a rapid overflight of the target area, as in typical airborne INSAR or LIDAR measurements, and thus the question of using a model to determine the relation between spatial and temporal information arises. Kennedy et al (2000b) considered the question of whether the Boussinesq model could be used as a bridge between two images of dynamic variables with small separation in time. Considering an artificial example where both $\mathbf{u}_\alpha$ and η are given at two times over a dense spatial image, they developed a realizable method in which the model is

initialized with the first image and an assumed bathymetry, and then integrated forward in time to the time of the second image. The mismatch between computed and measured dynamic variables at the time of the second image is used as a basis for iterative correction of the bathymetry. Kennedy et al showed that the iteration converged rapidly and that separations on the order of 1/4 to 1/3 of a dominant wave period were adequate. Subsequently, Misra et al (2000) have considered a more realistic case where one or more dynamic variables are missing.

6.2 Tsunami propagation and runup

An important and rapidly growing area of Boussinesq model application is in the modeling of the generation, propagation and runup of tsunamis. This process has traditionally been approached using models based on nonlinear shallow water equations (see, for example, Synolakis et al, 2002), but there are obvious advantages to using Boussinesq models, particularly in the better representation of vertical flow structure near source regions, a better prediction of wave crest geometry and crest disintegration during propagation over complex topography, and in the modeling of accumulated frequency dispersion effects in ocean-basin scale propagation problems. Applications of this sort are in their infancy, but will play a prominant role in the future. Lynett and Liu (2002) have presented an initial study of the generation of tsunamis due to bottom slumping, concentrating on one dimensional and symmetric two dimensional bottom motions. Watts et al (2002) have described a modeling system called *GEOWAVE*, which consists of a modified version of the *FUNWAVE* model coupled to a three-dimensional nearfield tsunami source model. Figure 22 shows an example calculation based on a slump-type source for the Papua New Guinea tsunami of July 17, 1998. The figure indicates maximum surface elevation occuring at each location in the modeled domain, and indicates runup and inundation of the shoreline facing the source region. Results of this study are preliminary, and detailed quantitative comparisons to estimated runup elevations in the field will be described elsewhere.

7 Conclusions

The development of Boussinesq models for application to coastal hydrodynamics problems has reached a level of maturity that would probably not have been expected a decade ago. The model formulation has been extended to allow for wave propagation in almost all finite water depths, rendering the notion of the models being only applicable in shallow water obsolete. A wide range of associated physical phenomena have been incorporated in model formulations, making it possible to apply Boussinesq model technology to the surfzone. The technology is also beginning to supplant the nonlinear shallow water equations (NLS) in a number of areas where the NLS has long been the dominant player; in calculation of wave runup and overtopping on coastal structures and in

calculation of tsunami propagation and inundation. In addition, the application of Boussinesq models to problems of coastal sediment transport (reviewed elsewhere in this volume) is just beginning. The long computational times involved in present calculations still hinder this line of research, but increasing computer capacity and speed will make it possible, in time, to approach the problem of morphological planform evolution with direct application of Boussinesq model codes.

It is apparent from several of the sections above that the existing versions of higher-accuracy Boussinesq models are dauntingly complex in form, and it becomes relevant to address the question of whether further development along these lines is warranted relative to direct utilization of the Navier Stokes equations. This concern is well placed. However, there is a great deal of room in numerical efficiency between the practical $O(\mu^2)$ models described above and any competing formulation of the Navier-Stokes or Euler equations in three dimensions, and thus the models described here are likely to be the basis for practical computations for a number of years. Indeed, the examples of Navier-Stokes based wave propagation calculations which are presently available (for example, Casulli, 1999 or Lin and Li, 2002) show results for the shoaling example of Beji and Battjes (1994) which are less accurate than corresponding Boussinesq calculations, even using $O(\mu^2)$ models for comparison. It is likely that the typical second-order accurate numerical schemes used in Navier-Stokes solvers to date are a limiting factor in obtaining accurate results, indicating a need for further development in this area.

Acknowledgements: The University of Delaware component of the work described here would not have been possible without the efforts of my students and colleagues, including Arun Chawla, Qin Chen, Tony Dalrymple, Mauricio Gobbi, Andrew Kennedy, Valeria Rego, Fengyan Shi, Ib Svendsen, Jayaram Veeramony and Ge Wei. This work has been supported by the Army Research Office, the Office of Naval Research, the National Science Foundation, and the NOAA Seagrant Program, and is presently supported by the National Ocean Partnership Program (NOPP).

References

Agnon, Y., Madsen, P. A. and Schäffer, H. A., 1999. A new approach to high-order Boussinesq models. Journal of Fluid Mechanics, Vol. 399, pp. 319-333.

Basco, D. R., 1983. Surfzone currents. Coastal Engineering, Vol. 7, pp. 331-355.

Beji, S. and Battjes, J. A., 1993. Experimental investigations of wave propagation over a bar. Coastal Engineering, Vol. 19, pp. 151-162.

Bowen, A. J. and Holman, R. A., 1989. Shear instabilites of the mean longshore current. 1. Theory. Journal of Geophysical Research, Vol. 94, pp. 18,023-18,030.

Brackbill, J. U. and Saltzman, J. S., 1982. Adaptive zoning for singular problems in two dimensions. Journal of Computational Physics, Vol. 46, pp. 342-368.

Casulli, V., 1999. A semi-implicit finite difference method for non-hydrostatic, free surface flows. International Journal for Numerical Methods in Fluids, Vol. 30, pp. 425-440.

Chawla, A. and Kirby, J. T., 2000. A source function method for generation of waves on currents in Boussinesq models. Applied Ocean Research, Vol. 22, pp. 75-83.

Chen, Q., Dalrymple, R. A., Kirby, J. T., Kennedy, A. B. and Haller, M. C., 1999. Boussinesq modeling of a rip current system. Journal of Geophysical Research, Vol. 104, pp. 20,617 - 20,637.

Chen, Q., Kirby, J. T., Dalrymple, R. A., Kennedy, A. B. and Chawla, A., 2000a. Boussinesq modeling of wave transformation, breaking and runup. II: 2D. Journal of Waterway, Port, Coastal and Ocean Engineering, Vol. 126, pp. 48-56.

Chen, Q., Kirby, J. T., Dalrymple, R. A., Kennedy, A. B., Thornton, E. B. and Shi, F., 2000b. Boussinesq modeling of waves and longshore currents under field conditions. Proceedings of the 27th International Conference on Coastal Engineering, Sydney, July 16-21, pp. 651-663.

Dingemans, M. W., 1997. Water Wave Propagation over Uneven Bottoms. Part 2 - Non-linear Wave Propagation. World Scientific, Singapore.

Dommermuth, D. G. and Yue, D. K. P., 1987. A high-order spectral method for the study of nonlinear gravity waves. Journal of Fluid Mechanics, Vol. 184, pp. 267-288.

Dugan, J. P., Piotrowski, C. C. and Williams, J. Z., 2001. Water depth and surface current retrievals from airborne optical measurements of surface gravity wave dispersion. Journal of Geophysical Research, Vol. 106, pp. 16,903-16,915.

Fenton, J. D., 1973. Some results for surface gravity waves in shear flows. Journal of the Institute of Mathematics and its Applications, Vol. 12, pp. 1-20.

Gobbi, M. F. and Kirby, J. T., 1999. Wave evolution over submerged sills: Tests of a high-order Boussinesq model. Coastal Engineering, Vol. 37, pp. 57-96.

Gobbi, M. F., Kirby, J. T. and Wei, G., 2000. A fully nonlinear Boussinesq model for surface waves. II. Extension to $O(kh^4)$. Journal of Fluid Mechanics, Vol. 405, pp. 181-210.

Haller, M. C. and Dalrymple, R. A., 2001. Rip current instabilities. Journal of Fluid Mechanics, Vol. 433, pp. 161-192.

Hommel, D., Shi, F., Kirby, J. T., Dalrymple, R. A. and Chen, Q., 2000. Modelling of a wave-induced vortex near a breakwater. Proceedings of the 27th International Conference on Coastal Engineering, Sydney, July 16-21 pp. 2318-2330.

Hsiao, S.-C., Liu, P. L.-F. and Chen, Y., 2002. Nonlinear water waves propagating over a permeable bed. Proceedings of the Royal Society of London A, in press.

Kennedy, A. B, Chen, Q., Kirby, J. T., and Dalrymple, R. A., 2000a. Boussinesq modeling of wave transformation, breaking and runup. I: 1D. Journal of Waterway, Port, Coastal and Ocean Engineering, Vol. 126, pp. 39-47.

Kennedy, A. B., Dalrymple, R. A., Kirby, J. T. and Chen, Q., 2000b. Determination of inverse depths using direct Boussinesq modelling. Journal of Waterway, Port, Coastal and Ocean Engineering, Vol. 126, pp. 206-214.

Kennedy, A. B., Kirby, J. T., Chen, Q. and Dalrymple, R. A., 2001. Boussinesq-type equations with improved nonlinear performance. Wave Motion, Vol. 33, pp. 225-243.

Kennedy, A. B., Kirby, J. T. and Gobbi, M. F., 2002. Simplified higher order Boussinesq equations. 1: Linear simplifications. Coastal Engineering, Vol. 44, pp. 205-229.

Kirby, J. T. and Dalrymple, R. A., 1984. Surfzone Currents, by D. R. Basco - Discussion. Coastal Engineering, Vol. 8, pp. 387-392.

Kirby, J. T., 1997. Nonlinear, dispersive long waves in water of variable depth. In: Hunt, J. N. (Editor), Gravity Waves in Water of Finite Depth. Advances in Fluid Mechanics, Vol 10, pp. 55-125, Computational Mechanics Publications.

Kirby, J. T., Wei, G., Chen, Q., Kennedy, A. B. and Dalrymple, R. A., 1998. FUNWAVE 1.0. Fully nonlinear Boussinesq wave model. Documentation and user's manual. Report CACR-98-06, Center for Applied Coastal Research, Department of Civil and Environmental Engineering, University of Delaware.

Li, Y. S., Liu, S. X., Yu, Y.X. and Lai, G. Z., 1999. Numerical modeling of Boussinesq equations by finite element method. Coastal Engineering, Vol. 37, pp. 97-122.

Li, Y. S. and Zhan, J. M., 2001. Boussinesq-type model with boundary-fitted coordinate system. Journal of Waterway, Port, Coastal and Ocean Engineering, Vol. 127, pp. 152-160.

Lin, P. and Li, C. W., 2002. A σ-coordinate three-dimensional numerical model for surface wave propagation. International Journal for Numerical Methods in Fluids, Vol. 38, pp. 1045-1068.

Liu, P. L.-F., 1994. Model equations for wave propagations from deep to shallow water. In: Liu, P. L-F. (Editor), Advances in Coastal and Ocean Engineering, Vol. 1, pp. 125-157. World Scientific.

Lynett, P. J., Wu, T.-R. and Liu, P. L.-F., 2002. Modeling wave runup with depth-integrated equations. Coastal Engineering, in press.

Lynett, P. J. and Liu, P. L. F., 2002. A numerical study of submarine landslide generated waves and runup. Proceedings Royal Society of London A, in press.

Madsen, P. A., Murray, R. and Sørensen, O. R., 1991. A new form of Boussinesq equations with improved linear dispersion characteristics. Part 1. Coastal Engineering, Vol. 15, pp. 371-388.

Madsen, P. A., Sørensen, O. R. and Schäffer, H. A., 1997. Surfzone dynamics simulated by a Boussinesq type model. Part 1: Model description and cross-shore motion of regular waves. Coastal Engineering, Vol. 32, pp. 255-288.

Madsen, P. A. and Schäffer, H. A., 1998. Higher-order Boussinesq-type equations for surface gravity waves: derivation and analysis. Philosophical Transactions of the Royal Society of London A, Vol. 356, pp. 3123-3184.

Madsen, P. A. and Schäffer, H. A., 1999. Review of Boussinesq-type equations for surface gravity waves. In: Liu, P. L-F. (Editor), Advances in Coastal and Ocean Engineering, Vol. 5, pp. 1-94. World Scientific.

Madsen, P.A., Bingham, H. B. and Schaffer, H. A., 2002. Boussinesq-type formulations for fully nonlinear and extremely dispersive water waves: Derivation and analysis. Proceedings of the Royal Society of London A, in press.

Mase, H., 1995. Frequency downshift of swash oscillation compared to incident waves. Journal of Hydraulic Research, Vol. 33, pp. 397-411.

Misra, S., Kennedy, A. B., Kirby, J. T. and Dalrymple, R. A., 2000. Determining water depths from surface images using Boussinesq equations. Proceedings of the 27th International Conference on Coastal Engineering, Sydney, July 16-21, pp. 1197-1210.

Nwogu, O., 1993. Alternative form of Boussinesq equations for nearshore wave propagation. Journal of Waterway, Port, Coastal and Ocean Engineering, Vol. 119, pp. 618-638.

Nwogu, O. and Demirbilek, Z., 2001. BOUSS-2D: A Boussinesq wave model for coastal regions and harbors. ERDC/CHL TR-01-25, Coastal and Hydraulics Laboratory, USACOE Engineer Research and Development Center, , Vicksburg, MS.

Oltman-Shay, J., Howd, P. A. and Birkemeier, W. A., 1989. Shear instabilites of the mean longshore current. 2. Field observations. Journal of Geophysical Research, Vol. 94, pp. 18,031-18,042.

Özkan-Haller, H. T. and Kirby, J. T., 1997. A Fourier-Chebyshev collocation method for the shallow water equations including shoreline runup. Applied Ocean Research, Vol. 19, pp. 21-34.

Özkan-Haller, H. T. and Kirby, J. T., 1999. Nonlinear evolution of shear instabilities of the longshore current: A comparison of observations and computations. Journal of Geophysical Research, Vol. 104, pp. 25,953 - 25,984.

Peregrine, D. H., 1998. Surf zone currents. Theoretical and computational fluid dynamics, Vol. 10, pp. 295-309.

Rego, V. S., Kirby, J. T. and Thompson, D., 2001. Boussinesq waves on flows with arbitrary vorticity. Proceedings of the 4th International Symposium on Ocean Wave Measurement and Analysis, Waves'01, ASCE, San Francisco, September 2-6, pp. 904-913.

Roddier, D. and Ertekin, R. C., 1999. Diffraction and remodelization of solitons around a false wall. Chaos, Solitons and Fractals, Vol. 10, pp. 1221-1240.

Schäffer, H. A., Madsen, P. A. and Deigaard, R., 1993. A Boussinesq model for waves breaking in shallow water. Coastal Engineering, Vol. 20, pp. 185-202.

Schäffer, H. A.and Madsen, P. A., 1995. Further enhancements of Boussinesq-type equations. Coastal Engineering, Vol. 26, pp. 1-14.

Shen, C. Y., 2001. Constituent Boussinesq equations for waves and currents. Journal of Physical Oceanography, Vol. 31, pp. 850-859.

Shi, F., Dalrymple, R. A., Kirby, J. T., Chen, Q. and Kennedy, A., 2001a. A fully nonlinear Boussinesq model in generalized curvilinear coordinates. Coastal Engineering, Vol. 42, pp. 337-358.

Shi, F., Kirby, J. T., Dalrymple, R. A. and Chen, Q., 2001b. A curvilinear Boussinesq model and its application. Proceedings of the 4th International Symposium on Ocean Wave Measurement and Analysis, Waves'01, ASCE, San Francisco, September 2-6, pp. 844-853.

Shields, J. J. and Webster, W. C., 1988. On direct methods in water-wave theory. Journal of Fluid Mechanics, Vol. 197, pp. 171-199.

Sørensen, O. R., Schäffer, H. A. and Madsen, P. A., 1998. Surfzone dynamics simulated by a Boussinesq type model. Part III: Wave induced horizontal nearshore circulations. Coastal Engineering, Vol. 33, pp. 155-176.

Sørensen, O. R. and Sørensen, L. S., 2000. Boussinesq type modelling using unstructured finite element technique. Proceedings of the 27th International Conference on Coastal Engineering, Sydney, July 16-21, pp. 190-202.

Stockdon, H. F. and Holman, R. A., 2000. Estimation of wave phase speed and nearshore bathymetry from video imagery. Journal of Geophysical Research, Vol. 105, pp. 22,105-22,033.

Svendsen, I. A., 1984. Wave heights and setup in a surfzone. Coastal Engineering, Vol. 8, pp. 303-329.

Svendsen, I. A. and Putrevu, U., 1994. Nearshore mixing and dispersion. Proceedings of the Royal Society of London A, Vol. 445, pp. 1-16.

Svendsen, I. A., Veeramony, J., Bakunin, J. and Kirby, J. T., 2000. The flow in weak turbulent hydraulic jumps. Journal of Fluid Mechanics, Vol. 418, pp. 25-57.

Synolakis, C. E., Bardet, J.-P., Borrero, J. C., Davies, H. L., Okal, E. A., Silver, E. A., Sweet, S. and Tappin, D. R., 2002. The slump origin of the 1998 Papua New Guinea tsunami. Proceedings of the Royal Society of London A, Vol. 458, pp. 763-789.

Tanaka, M., 1986. The stability of solitary waves. Physics of Fluids, Vol. 29, pp. 650-655.

Tao, J., 1984. Numerical modelling of wave runup and breaking on the beach. Acta Oceanologica Sinica, Vol. 6, pp. 692-700 (in Chinese).

Veeramony, J. and Svendsen, I. A., 2000. The flow in surf-zone waves. Coastal Engineering, Vol. 39, pp.93-122.

Walkley, M. and Berzins, M., 1999. A finite element method for the one-dimensional extended Boussinesq equations. International Journal for Numerical Methods in Fluids, Vol. 29, pp. 143-157.

Warsi, Z. U. A., 1993. Fluid Dynamics: Theoretical and Computational Approaches. CRC Press, Boca Raton.

Watts, P., Grilli, S. T. and Kirby, J. T., 2002. Coupling 3D tsunami generation with Boussinesq tsunami propagation. presentation at the 27th European Geophysical Society General Assembly, Nice, April 21-26.

Wei, G. and Kirby, J. T., 1995. A time-dependent numerical code for extended Boussinesq equations. Journal of Waterway, Port, Coastal and Ocean Engineering, Vol. 120, pp. 251-261.

Wei, G., Kirby, J. T., Grilli, S. T. and Subramanya, R., 1995. A fully nonlinear Boussinesq model for surface waves. I. Highly nonlinear, unsteady waves. Journal of Fluid Mechanics, Vol. 294, pp. 71-92.

Wei, G., Kirby, J. T. and Sinha, A., 1999. Generation of waves in Boussinesq models using a source function method. Coastal Engineering, Vol. 36, pp. 271-299.

Woo, S.-B. and Liu, P. L.-F., 2001. A Petrov-Galerkin finite element model for one-dimensional fully non-linear and weakly dispersive wave propagation. International Journal for Numerical Methods in Fluids, Vol. 37, pp. 541-575.

Yoon, S. B. and Liu, P. L.-F., 1989. Interactions of currents and weakly nonlinear water waves in shallow water. Journal of Fluid Mechanics, Vol. 205, pp. 397-419.

Zelt, J. A., 1991. The runup of nonbreaking and breaking solitary waves. Coastal Engineering, Vol. 15, pp. 205-246.

List of Symbols

a_0	wave amplitude scale
c	wave phase speed
c_m	coefficient in expression for vorticity in Smagorinsky scheme
f	bottom friction factor
g	gravitational constant
$k, \mathbf{k}$	scalar wavenumber, vector wavenumber
k_0	wavenumber (or inverse wavelength) scale
$h(\mathbf{x})$	still water depth
h_0	water depth scale
$H(\mathbf{x},t) = h + \delta\eta$	total instantaneous water depth
$\mathbf{M}(\mathbf{x},t)$	horizontal depth-integrated volume flux vector
Q	horizontal volume flux in 1-D theory
$\mathbf{R_b}, \mathbf{R_s}, \mathbf{R_f}$	wave breaking, subgrid mixing and bottom friction terms in orizontal momentum equations
t	time coordinate
$\mathbf{u} = (u, v)$	horizontal velocity vector
$\mathbf{u}_\alpha = (u_\alpha, v_\alpha)$	horizontal velocity at reference elevation
$\tilde{\mathbf{u}} = (\tilde{u}, \tilde{v})$	weighted horizontal velocity in Gobbi's theory
$\mathbf{V_1}, \mathbf{V_2}$	$O(\mu^2)$, dispersive terms in Boussinesq equations
w	vertical velocity
$\mathbf{x} = (x, y)$	horizontal coordinate
$\Delta x, \Delta y$	finite difference grid spacings
z	vertical coordinate
z_a, z_b, z_α	reference elevations
α	dispersion enhancement parameter, see (17)
β	weighting factor in theory of Gobbi
$\delta = a_0/h_0$	nonlinearity parameter
$\eta(\mathbf{x},t)$	water surface elevation
$\mu = k_0 h_0$	dispersion parameter
ν	viscosity coefficient
ν_b	eddy viscosity coefficient in Zelt-type breaker model
ν_s	eddy viscosity coefficient in Smagorinsky subgrid scheme
ω	wave angular frequency
$\boldsymbol{\omega}, \boldsymbol{\omega_1}$	total and $O(\mu^2)$ contribution to vertical vorticity vector
$\phi(\mathbf{x}, z, t)$	velocity potential
$\phi_a, \phi_b, \phi_\alpha(\mathbf{x}, t)$	velocity potential at reference elevations
$\tilde{\phi}(\mathbf{x}, t)$	weighted velocity potential in Gobbi's theory
$\phi^{(n)}$	components of series solution for ϕ
$\psi(x, z, t)$	scalar stream function
ξ	scalar magnitude of horizontal vorticity
$\boldsymbol{\xi} = (\xi_x, \xi_y)$	projection of total vorticity vector in horizontal plane
ζ	parameter in Kennedy's moving reference elevation model
$\nabla = \left(\frac{\partial}{\partial x}, \frac{\partial}{\partial y}\right)$	horizontal gradient operator

List of Figures

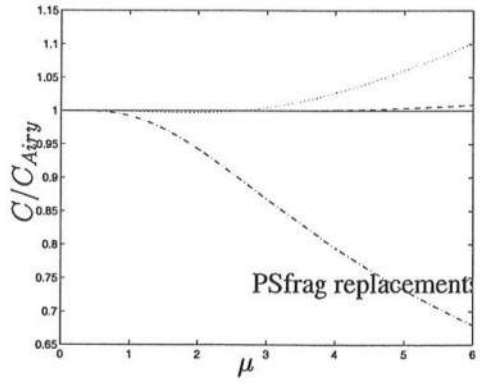

Figure 1: Ratio of model linear phase speed c to exact linear phase speed c_{Airy} given by (13). Standard Boussinesq dispersion with $\alpha = -1/3$ in (16) (dash-dot); optimized $O(\mu^2)$ dispersion based on the (2,2) Pade approximant with minimization of phase speed errors to obain $\alpha = -0.39$ in (16), following Nwogu (1993) (dotted); $O(\mu^4)$ dispersion based on (4,4) Pade approximant in (31) (dash). (From Gobbi et al, 2000)

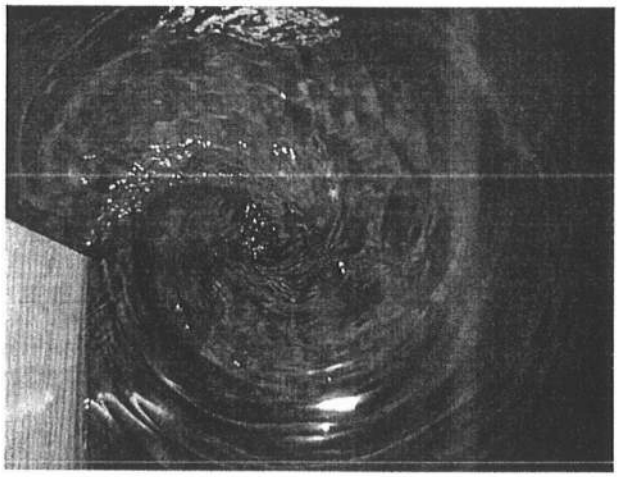

Figure 2: Shed vortex formed during passage of solitary wave past a vertical wall. (From Hommel, L., Shi, F., Kirby, J. T., Dalrymple, R. A. and Chen, Q., "Modelling of a wave-induced vortex near a breakwater", Proc. 27th Intl. Conf. Coastal Engrng., ASCE, Sydney, July 16-21, 2318-2330,2000. Reproduced with permission of ASCE.)

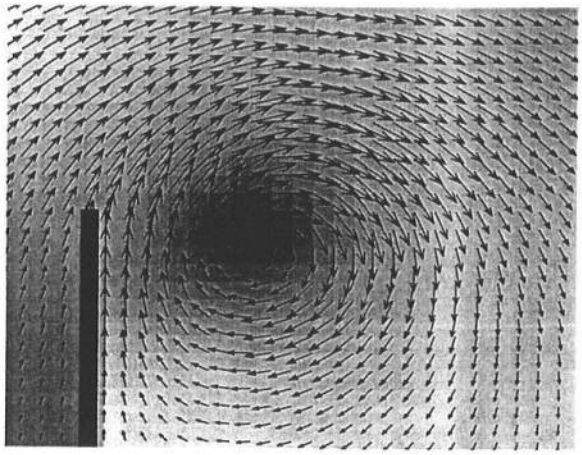

Figure 3: Calculated velocity field corresponding to vortex in Figure 2. (From Hommel, L., Shi, F., Kirby, J. T., Dalrymple, R. A. and Chen, Q., "Modelling of a wave-induced vortex near a breakwater", Proc. 27th Intl. Conf. Coastal Engrng., ASCE, Sydney, July 16-21, 2318-2330,2000. Reproduced with permission of ASCE.).

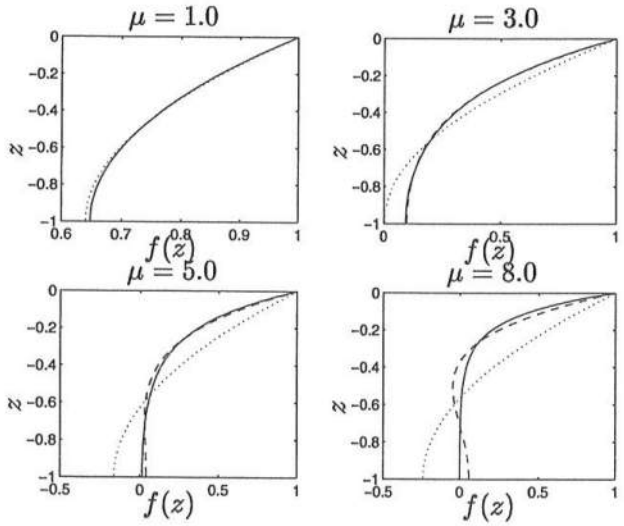

Figure 4: Normalized vertical profile of linear horizontal velocity at four values of μ. Exact linear solutions (solid), $O(\mu^2)$ approximate solution (dot), $O(\mu^4)$ approximate solution (dash) (From Gobbi et al, 2000)

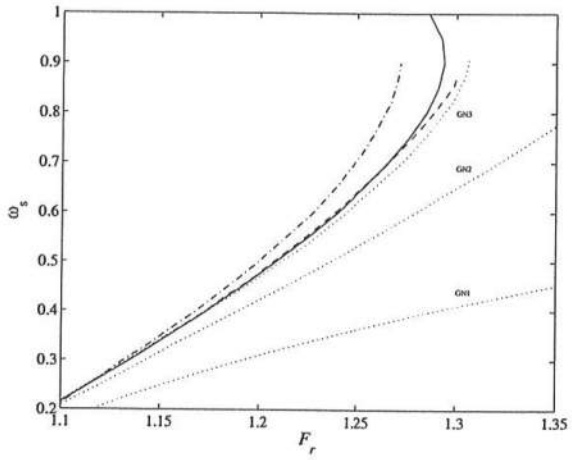

Figure 5: ω_s vs. phase speed for solitary waves. Exact (solid line), Gobbi et al (dash), Wei et al (dash-dot), Shields and Webster (dot). (From Gobbi et al, 2000)

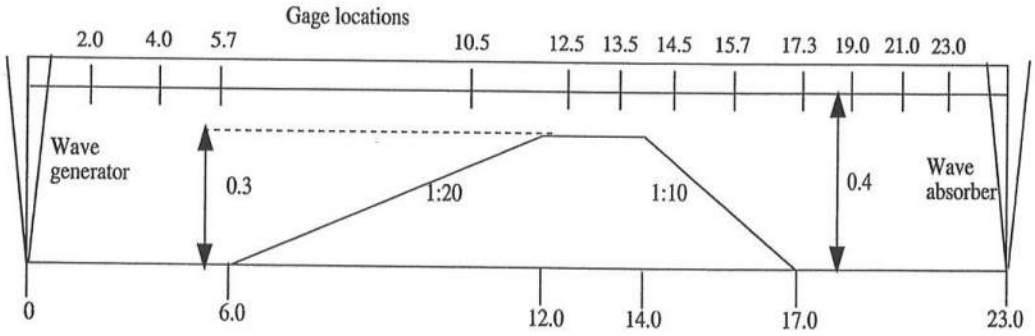

Figure 6: Sketch of wave flume in Delft experiments. All dimensions in (m). (From Gobbi and Kirby, 1999)

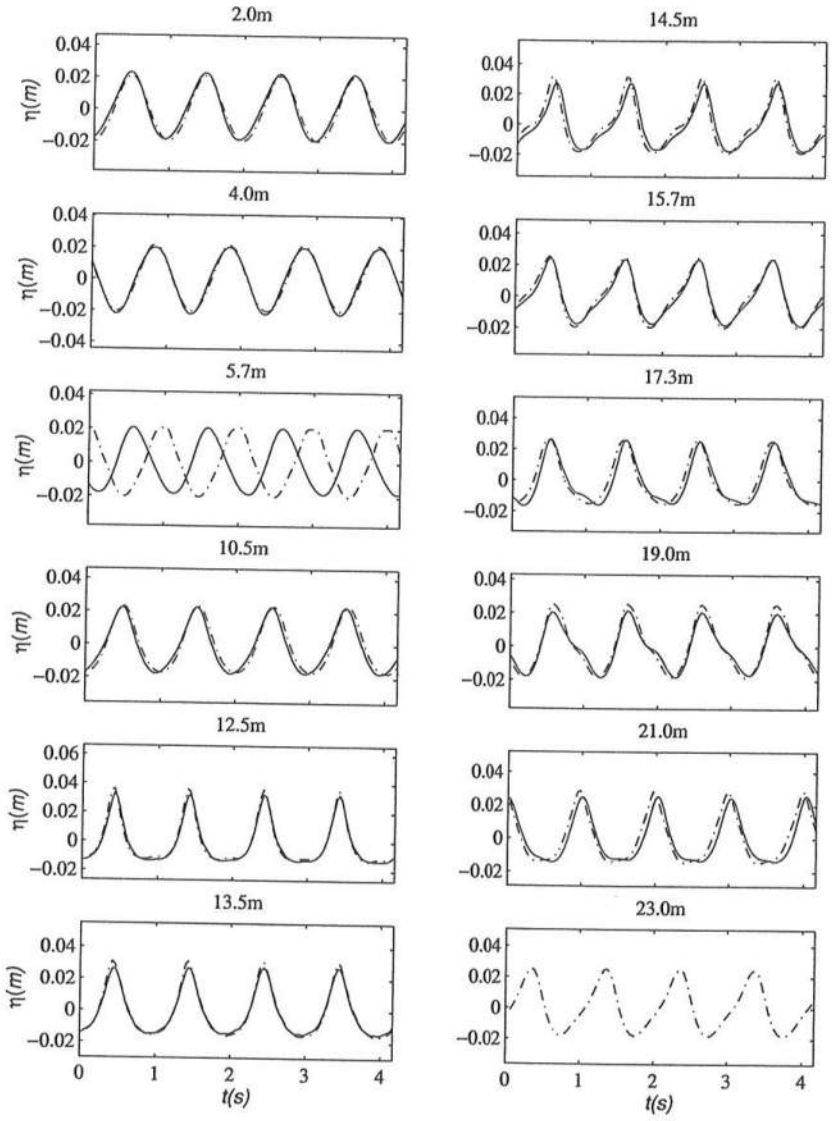

Figure 7: Comparisons of free surface displacement for case (c) of Delft experimental data at various gage locations. Model of Gobbi and Kirby (dash-dot), data (solid). (From Gobbi and Kirby, 1999)

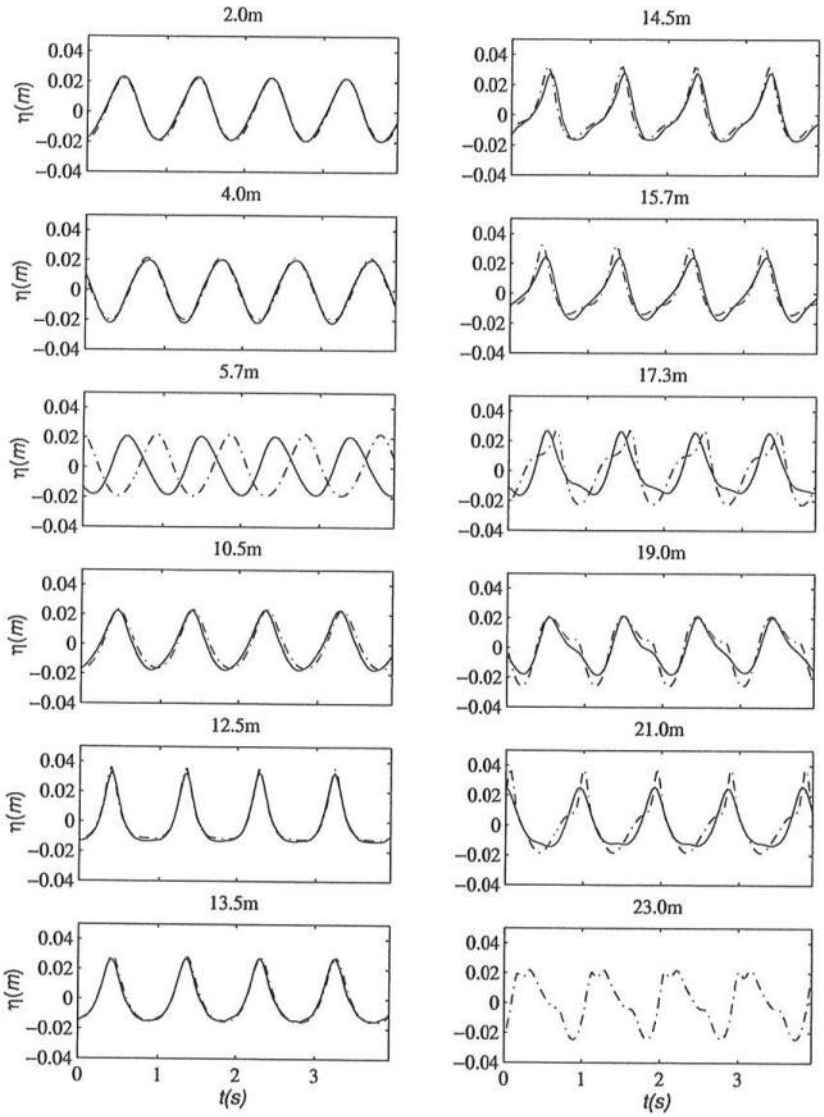

Figure 8: Comparisons of free surface displacement for case (c) of Delft experimental data at various gage locations. Model of Wei et al (dash-dot), data (solid). (From Gobbi and Kirby, 1999)

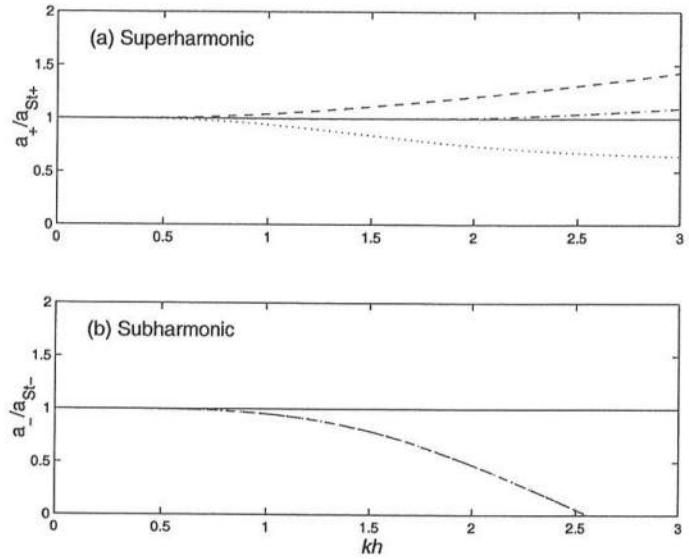

Figure 9: Self interaction superharmonics (a) and subharmonics (or setdown) (b) relative to the Stokes solution for the fully dispersive problem. Original Wei et al theory (dash), constant σ level theory (dot), optimized moving z_α theory (dash-dot). (From Kennedy et al, 2001)

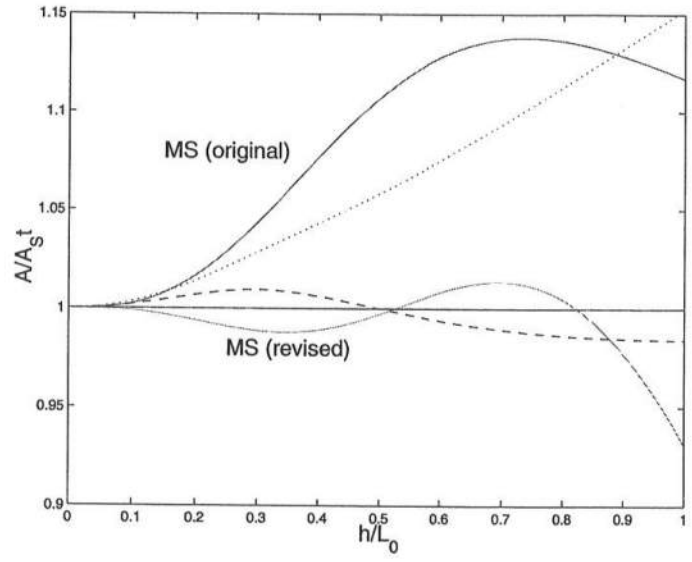

Figure 10: Integrated shoaling amplitudes for shore normal waves. (dash) Model optimized by coefficient choice alone, (dash-dot) model optimized by operator rearrangement and coefficient choice (obscured behind level line), (dot) linearized model of Nwogu (1993) or Wei et al (1995), plus results from Madsen and Schäffer (1998). (From Kennedy et al, 2002)

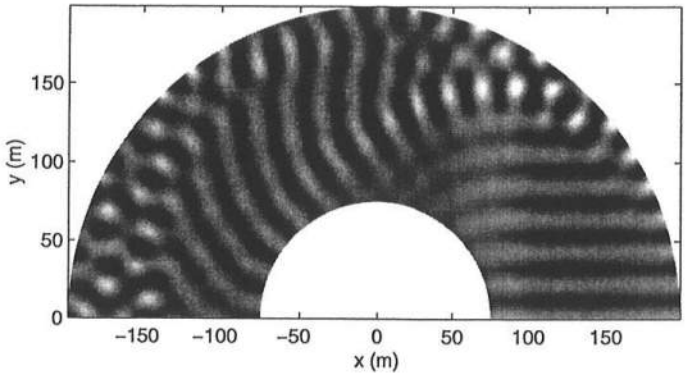

Figure 11: An example of initially plane wave propagation into a circular channel of constant depth. Boundary fitted coordinate system. (From Shi et al, 2001a)

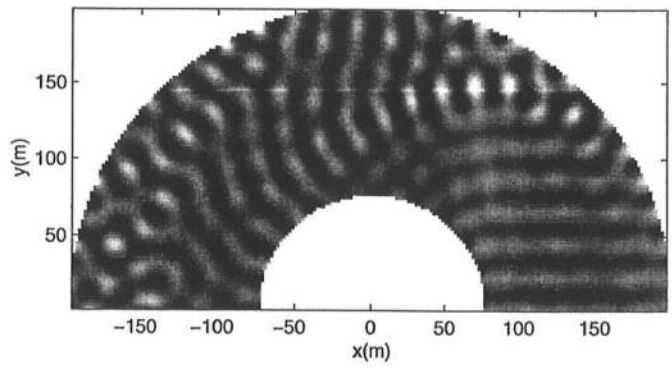

Figure 12: Example of 11 repeated on a Cartesian grid with stair-step boundaries. Note the appearance of spurious reflected components close to the incident wave entrance on the right. (from Shi et al, 2001a)

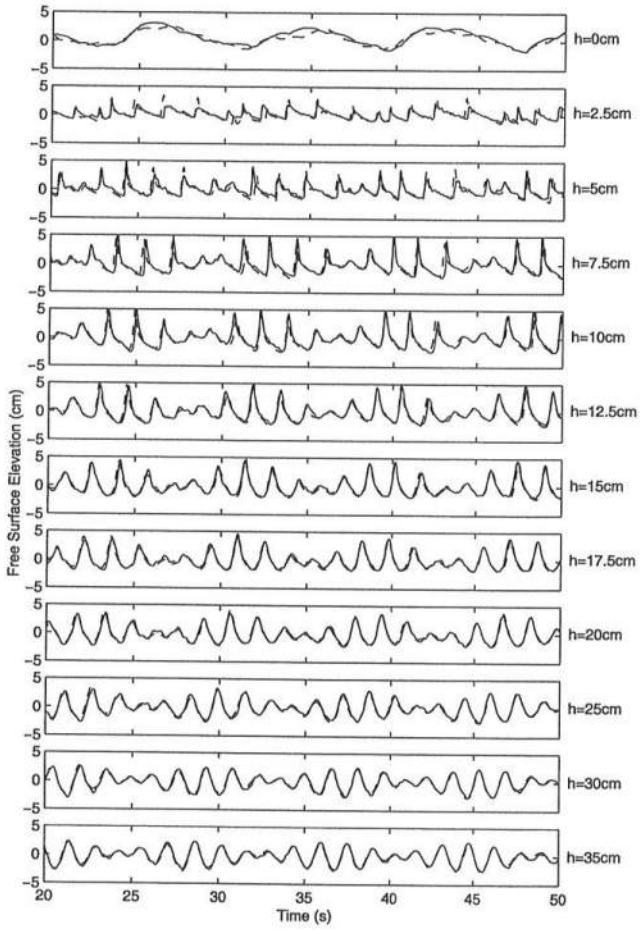

Figure 13: Computed (dash line) and measured (solid line) free surface elevations and shoreline runup for a bichromatic wave train shoaling on a plane beach. Data from Mase (1995). (From Kennedy, A. B, Chen, Q., Kirby, J. T., and Dalrymple, R. A., "Boussinesq modeling of wave transformation, breaking and runup. I: One dimension", *J. Waterway, Port, Coastal and Ocean Engrng.*, 126, 39-47, 2000a. Reproduced with permission of ASCE.)

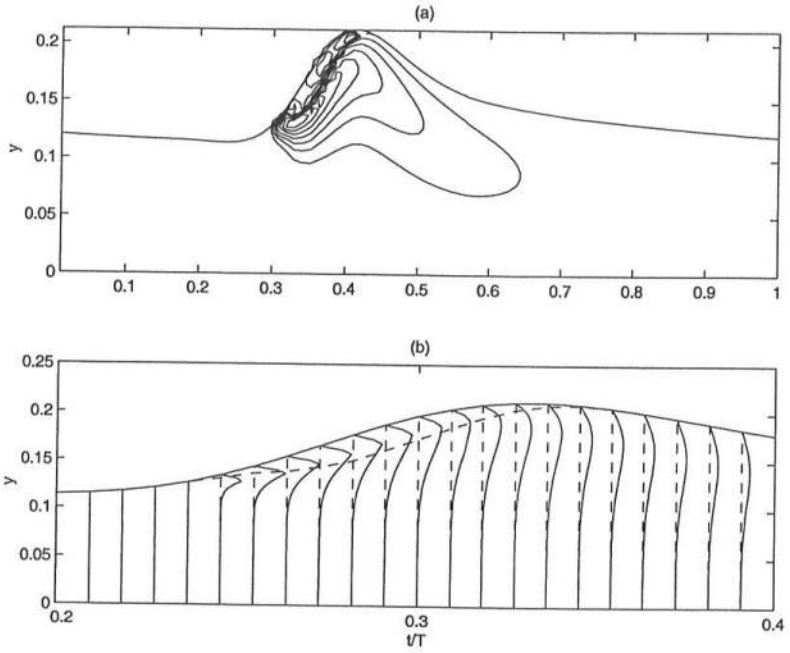

Figure 14: (a) Contours of vorticity at $h = 14.29$ cm. (b) Vertical profiles of vorticity under the roller and behind the crest at $h = 14.29$ cm. The ordinate $y = h + z$ is zero at the bottom. (From Veeramony and Svendsen, 2000)

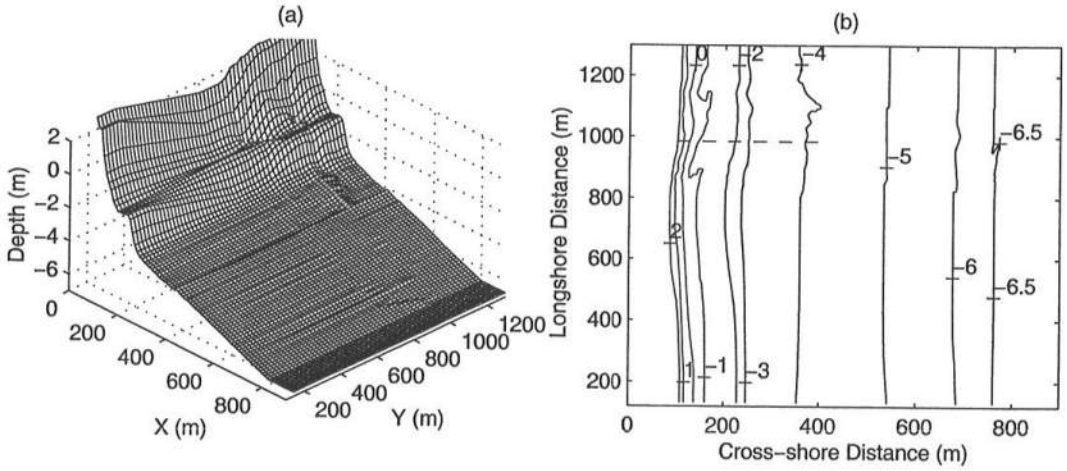

Figure 15: The bathymetry at the Field Research Facility, Duck, NC, Oct. 10, 1992: (a) topography, (b) depth contours. (from Chen, Q., Kirby, J. T., Dalrymple, R. A., Kennedy, A. B., Thornton, E. B. and Shi, F., "Boussinesq modeling of waves and longshore currents under field conditions", *Proc. 27th Intl. Conf. Coastal Engrng.*, ASCE, Sydney, July 16-21, 651-663, 2000b. Reproduced with permission of ASCE.)

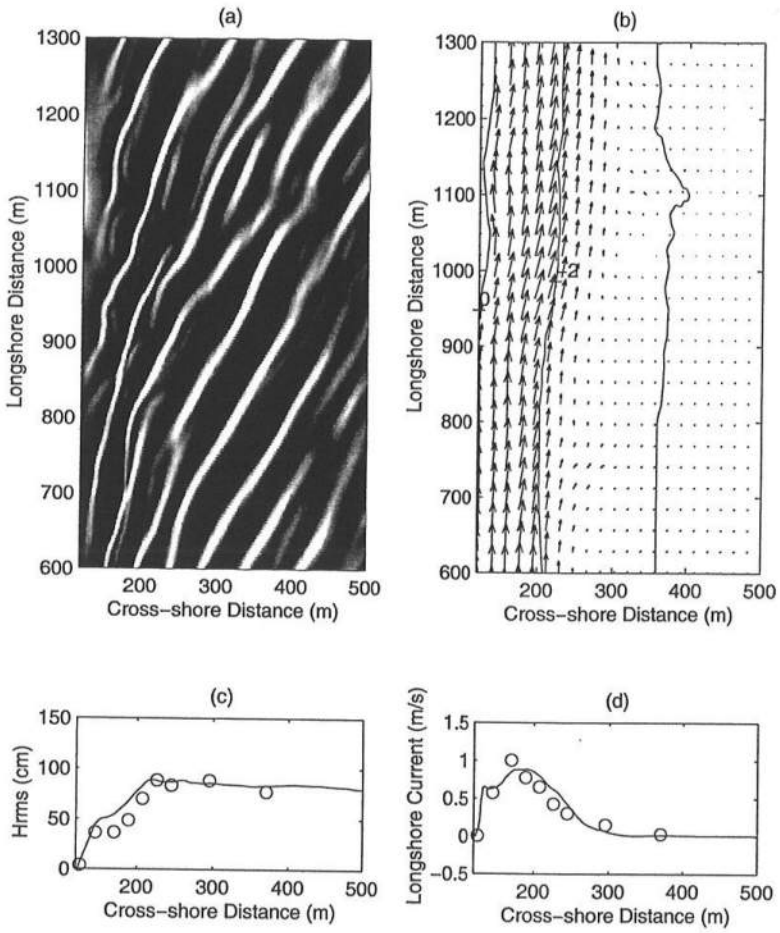

Figure 16: Model results: (a) snapshot of computed free surface elevation, light areas indicate wave crests; (b) computed time-averaged longshore current. (From Chen, Q., Kirby, J. T., Dalrymple, R. A., Kennedy, A. B., Thornton, E. B. and Shi, F., "Boussinesq modeling of waves and longshore currents under field conditions", *Proc. 27th Intl. Conf. Coastal Engrng.*, ASCE, Sydney, July 16-21, 651-663, 2000b. Reproduced with permission of ASCE.)

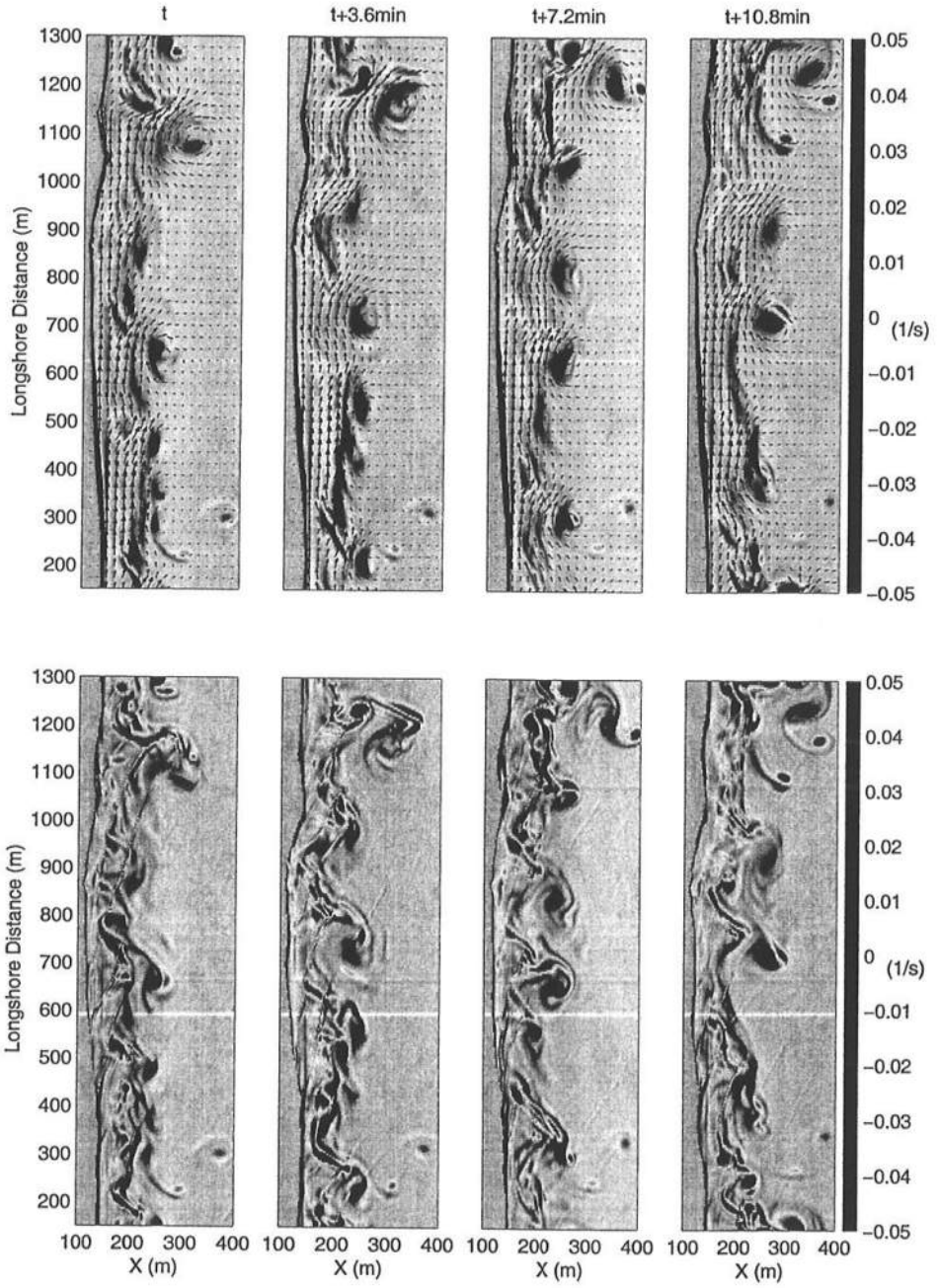

Figure 17: Time sequence of vorticity field, indicating presence of shear waves. Top panels display velocities and vorticity averaged over ten peak wave periods. Bottom panels display instantaneous vorticity. (from Chen, Q., Kirby, J. T., Dalrymple, R. A., Kennedy, A. B., Thornton, E. B. and Shi, F., "Boussinesq modeling of waves and longshore currents under field conditions", *Proc. 27th Intl. Conf. Coastal Engrng.*, ASCE, Sydney, July 16-21, 651-663, 2000b. Reproduced with permission of ASCE.)

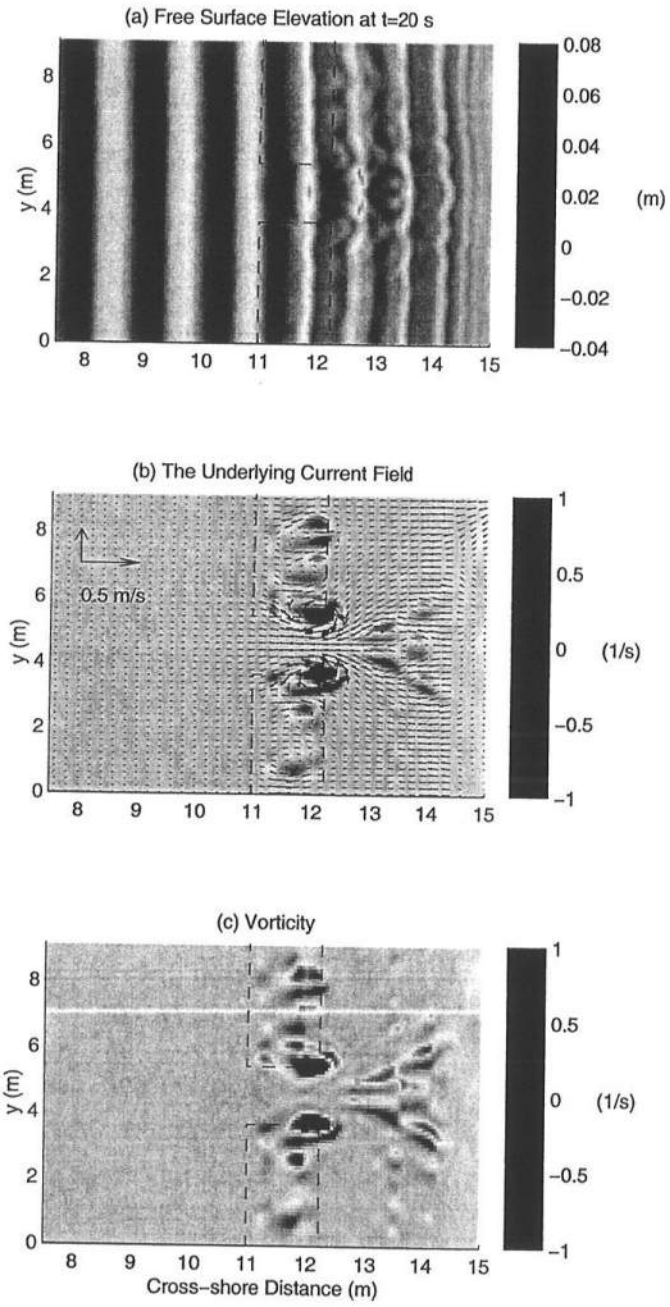

Figure 18: A snapshot of (a) the computed free surface elevation, (b) the underlying current field and associated mean vorticity, and (c) the instantaneous vorticity field at $t = 20s$, shortly after initiation of wave breaking over the longshore bar. Dashed lines indicate outline of longshore bar geometry in the laboratory. (From Chen et al, 1999, copyright [1999] by the American Geophysical Union)

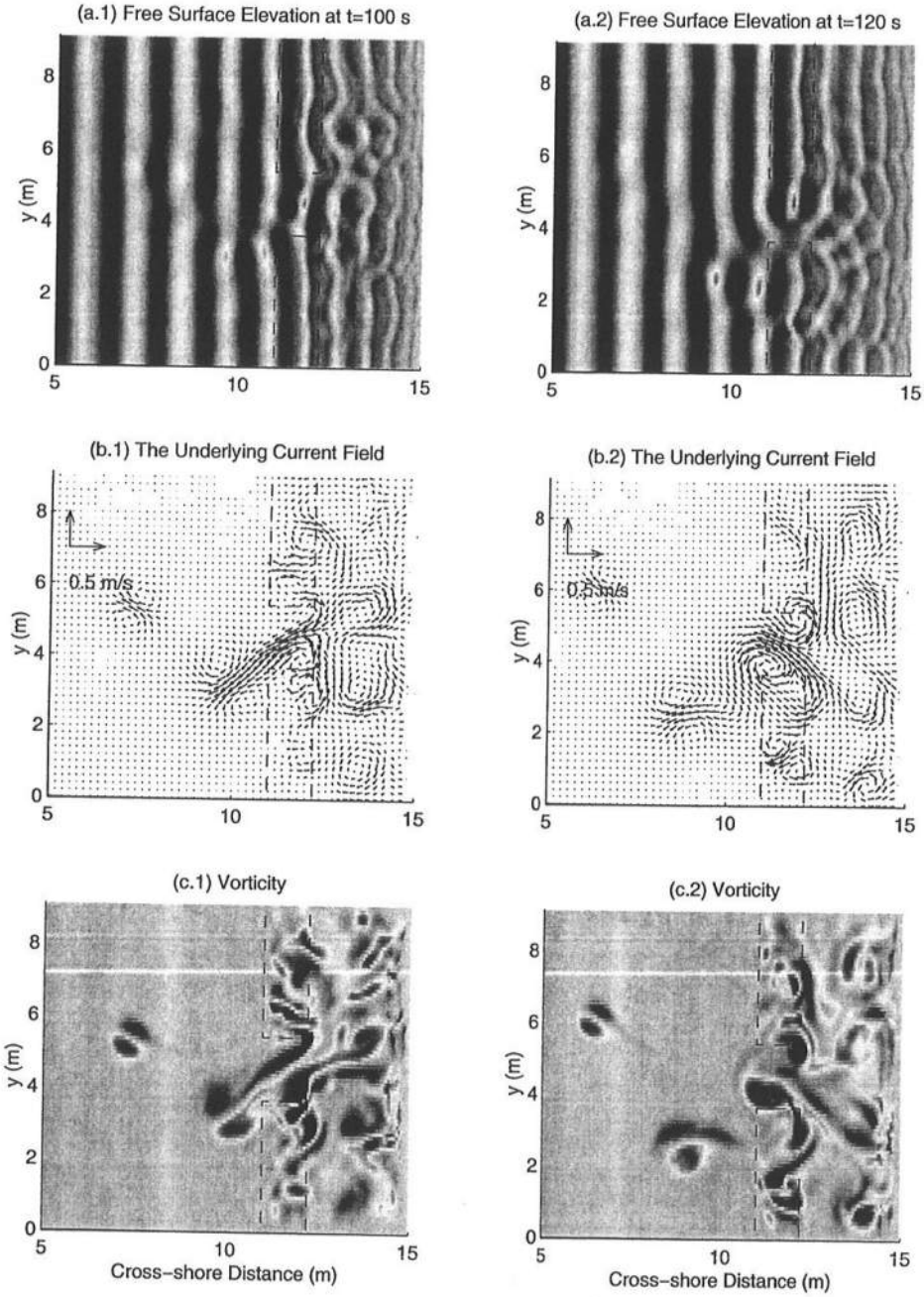

Figure 19: Snapshots of (a) the computed free surface elevation, (b) the underlying current field, and (c) vorticity at (left) $t = 100s$ and (right) $t = 120s$, illustrating unsteady behavior of rip current jet. (From Chen et al, 1999, copyright [1999] by the American Geophysical Union)

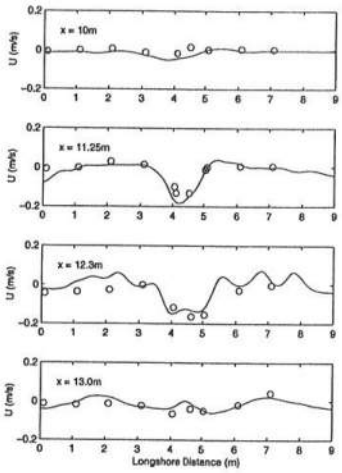

Figure 20: Comparison of computed (solid lines) and measured (circles) cross-shore mean velocity, resulting from time averages of velocities in the unsteady rip current illustrated in Figures 18 and 19. (From Chen et al, 1999, copyright [1999] by the American Geophysical Union)

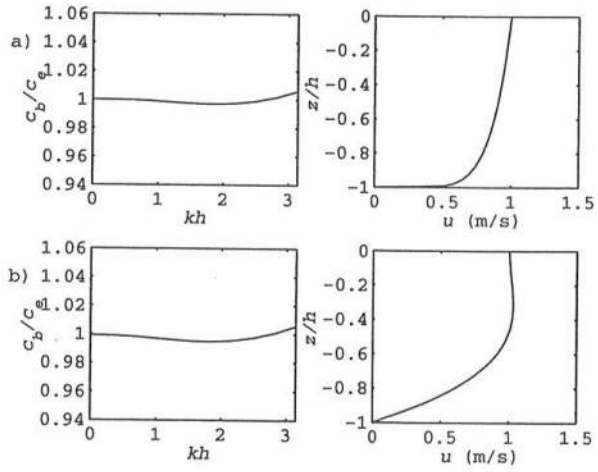

Figure 21: Normalized phase velocity (model phase velocity c_b divided by exact phase velocity c_e calculated from the Rayleigh equation) and associated current profiles: a) 1/7 power law, b) cubic polynomial. (From Rego, V. S., Kirby, J. T. and Thompson, D., "Boussinesq waves on flows with arbitrary vorticity", *Proceedings of the 4th International Symposium on Ocean Wave Measurement and Analysis, Waves'01*, ASCE, San Francisco, September 2-6, 904-913, 2001. Reproduced with permission of ASCE.)

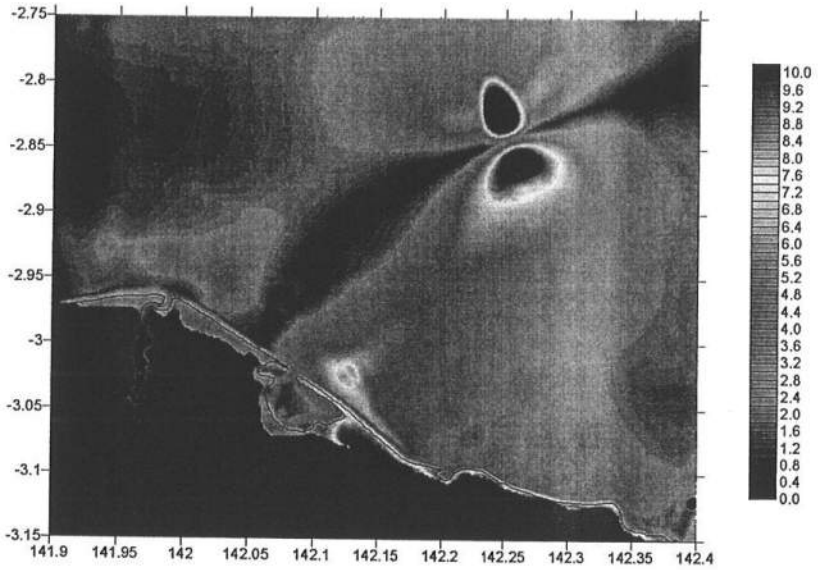

Figure 22: Model estimates of maximum local water surface elevations during July 17, 1998 Papua New Guinea tsunami event. Slump region is in vicinity of strong surface displacements offshore (upper right in picture). Shoreline is indicated by black line. Results indicate inundation beyond the mean shoreline, with runup amplitudes in excess of 10 meters in the region East of Sissano Lagoon, the main embayment in the figure. (after Watts et al, 2002)